ADVANCED MATERIALS TECHNOLOGIES
www.advmattechnol.de

A Review on Microreactor Design for Effective Fischer–Tropsch Process Intensification

Yangjun Wei, Lukas Thum, Avela Kunene, Daniel Amkreutz, Rutger Schlatmann, and Sonya Calnan*

Microreactors have high potential to achieve isothermal reaction conditions, short diffusion lengths as well as narrow residence time distributions, and thus, are very favorable for process intensification. In this review, experiments and simulation experiences on microreactors with cross sections of 10^{-2}–10^{1} mm for Fischer–Tropsch (FT) Synthesis are summarized, with a focus on reducing temperature and concentration gradients while maintaining a low pressure drop and sufficient FT liquid product removal. Using distinctions between packed-bed and wash-coated microreactors, four design aspects including heat transfer, mass transfer, pressure drop, residence, and contact time for microchannel/-tube and micromonolith/-structured versions are discussed, and the corresponding dimension, material- and operation-relevant parameters are investigated. Additional attention is also devoted to transferable benefits of microreactors to other syngas-related processes. Furthermore, limitations and challenges in experiments and simulations are noted, and future directions for investigations of microreactor design are suggested.

1. Introduction

The constantly increasing energy demand nowadays has become a main concern for economic growth and social development, while, on the other hand, the greenhouse gas (GHG) emissions from the use of fossil fuels cause a grand challenge of global warming.[1] Therefore, the decarbonization of energy systems and efficient energy utilization are urgently needed. According to the energy strategy of the European Union (EU), the GHG emissions are to be reduced by 80–95% from 1990 levels by 2050.[2]

To meet the demands of energy decarbonization, efficient utilization, storage, and mobility, various routes of X-to-X (XtX) are described in the literature in attempts to mitigate GHG emissions. Amongst many is power-to-X (PtX), which is characterized by converting electrical power and carbon source to gaseous or liquid fuels or chemicals,[3] X-to-liquid (XtL), which converts renewable carbon sources (e.g., biomass) to liquid fuels or chemicals,[4] are emerging technologies that have become a frontier area of research in recent years. Summarized in **Figure 1** are the possible flows of energy transformation, which are in line with sustainability goals.

Amongst many, Fischer–Tropsch synthesis (FTS) plays an important role in converting sustainable carbon sources to hydrocarbons, which is a typical gas-to-liquids (GtL) technology. Even though FTS was developed in the 1920s, this technology remains relevant to date with growing interest due to its agnostic nature regarding carbon sources such as feedstock (e.g., fossil fuels, renewables, biomass, organic/carbonaceous wastes, etc.). From this process a wide product spectrum of hydrocarbons (*n*-alkanes, *n*-alkenes) and oxygenates can be achieved, as illustrated following.

$$n\mathrm{CO} + (2n+1)\,\mathrm{H_2} \rightarrow \mathrm{C}_n\mathrm{H}_{2n+2} + n\mathrm{H_2O} \quad (1)$$

$$n\mathrm{CO} + (2n)\,\mathrm{H_2} \rightarrow \mathrm{C}_n\mathrm{H}_{2n} + n\mathrm{H_2O} \quad (2)$$

$$\mathrm{CO} + \mathrm{H_2O} \leftrightarrow \mathrm{CO_2} + \mathrm{H_2} \quad (3)$$

However, FTS is a highly exothermic reaction with typically $\Delta H_{\mathrm{STP}} = -165$ [kJ·mol^{-1}], varied according to product selectivity, which will strongly determine the chain growth probability. Thus, hot spots and operational runaway may have a negative influence on the product profile. Therefore, better heat control and heat removal are essential, and enormous attentions are drawn to this regard, aiming at high selectivity for targeted hydrocarbons.[5] Depending on the operating scale, heat management can become a challenge, particularly at a large industrial scale,[6,7] as this can induce pronounced catalyst sintering, which may ultimately lead

Y. Wei, L. Thum, A. Kunene, D. Amkreutz, R. Schlatmann, S. Calnan
PVcomB/Helmholtz-Zentrum Berlin für Materialien und Energie GmbH
12489 Berlin, Germany
E-mail: yangjun.wei@helmholtz-berlin.de
R. Schlatmann
HTW Berlin–University of Applied Sciences
12459 Berlin, Germany
S. Calnan
Loughborough University
Loughborough, Leicestershire LE11 3TU, UK

The ORCID identification number(s) for the author(s) of this article can be found under https://doi.org/10.1002/admt.202501557

DOI: 10.1002/admt.202501557

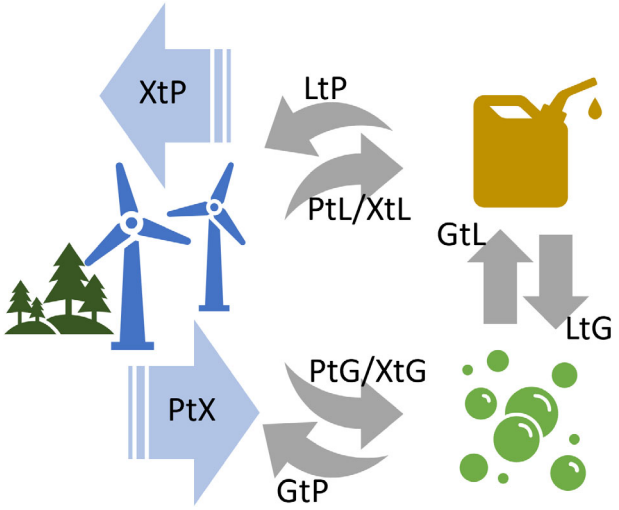

Figure 1. Schematic of various routes of X-to-X (XtX). P: power; L: liquid energy; G: gaseous energy; X: liquid or gaseous energy.

to catalyst deactivation.[8] However, the efficiency of FTS process is not limited to heat management only, parameters such as mass transfer, hydrodynamics (which include, but are not limited to, pressure drop and residence time distribution) also form an integral aspect in achieving an efficient industrial process. Exemplary mass transfer phenomena between gas–gas, gas–liquid, liquid–liquid, gas–solid, and liquid–solid should be considered. As such this makes FTS rather a complex process. Using FTS process as a model study can form a basis for understanding other relatively less complex gas–solid reactions, e.g., Sabatier reaction $\Delta H_{STP} = -165$ [kJ·mol^{-1}], steam reforming of methane $\Delta H_{STP} = 206.1$ [kJ·mol^{-1}].

To bring heat transfer, mass transfer, and hydrodynamics into consideration, reactor design is able to form an essential aspect that may unlock the full potential of this process. To date, depending on the mobility of the catalyst, FTS reactors can be categorized as fixed-bed (FB) reactors (e.g., monolith and microstructured reactors, where the catalyst is stationary in the reactor), slurry bed (SB) reactors and circulating fluidized bed (CFB) reactors.[9] In an FB the catalyst bed is typically packed in a defined reactor position while in a SB or CFB the catalyst is constantly well-mixed within the whole reactor. This means that during FTS operation, for FB the heat generation is localized where the catalyst bed is stationed, and this may cause catalyst sintering, then ultimately deactivate the catalyst.[10,11] Besides, pressure drop of FB is crucial in the industrial applications to reduce the compression costs,[9] and thus, high pressure drops make the reactor less flexible to be scaled up. On the other hand, SB has the advantages of temperature uniformity due to the well-mixing nature of the catalyst within the reactor, however, the separation of the catalyst and the liquid products remains non-trivial.[12] Furthermore, both SB and CFB require significant agitation power to keep the catalyst particles suspended, which can increase operating costs.[12] Whereas microreactors have become a rapidly developing reactor branch and are also distinguished by their small/micro dimension. For this, typically, the hydraulic diameter d_h which describes cross-sectional diameter of the reactor and is given by

$$d_h = \frac{4A}{P} \tag{4}$$

where A is the cross-sectional area of the flow [m^2] and P is the wetted perimeter of the cross-section [m]. Accordingly, FTS reactors can be categorized as industrial/large-, and small/micro scale. Exemplary large-scale FB, SB, and CFB plants (standard GtL production: 1000–2000 barrels per day (BPD)) for FTS have been constructed by Sasol (South Africa, Qatar, and Nigeria), PetroSA (South Africa), Shell (Malaysia and Qatar), Synfuels China (China), Yitai CTL Plant (China), Shenhua ICL (China), etc.[5] Typically, their cross-sectional hydraulic diameters (d_h, see (Equation 4)) are >> 10^1 [mm]. Conversely, an increasing number of FTS microchannel reactors were constructed – some of the most common ones by Velocys, Inc.,[13] KOGAS,[14] Ajou University,[15] and INERATEC GmbH[16] (detailed in Table 5). The integrated FTS pilot-scale microchannel reactors, with a capacity of ≈1 BPD, are able to achieve CO conversion of ≈70% and C_{5+} selectivity of ≈80%, demonstrating their comparability to commercial FB FTS reactors of similar processing capacity (28–44 BPD).[17] Besides, a catalytic microreactor can provide a specific external surface area (square meters of catalyst surface per cubic meter reactor volume) of approximately 2–5 × 10^4 [m^2·m^{-3}], while a traditional reactor 0.1–1 × 10^3 [m^2·m^{-3}].[18] Therefore, micro-scale reactors have garnered increasing interest not only because of their inherent advantages of short mass diffusion lengths, small concentration/temperature gradients but also their high potential for process intensification.[5,14,19] Moreover, micro-scale reactors are highly integrated, compact, portable and safe, making them suitable for many applications such as offshore and remote production facilities.[20] Additionally, microreactors enable the safe use of highly active catalysts,[21] and thus, have driven a recent increase in interest especially for FTS process. Here, d_h is in a range of 10^{-2}–10^1 [mm] for a typical microreactor, maintaining the advantages for heat and mass transfer, where d_h may indicate the size of the parallel unit (e.g., of microchannel reactor), structure inserted in the reactor or reactor itself. The microreactors within this range are focused in the following sections of this review.

The literature contains numerous investigations on catalyst development and the use of conventional reactors (i.e., FB, SB and CFB) for FTS.[5,22–24] However, very limited works focus on neither simultaneous design on heat and mass transfer as well as hydrodynamics for microreactors nor optimization for the conflicting reactor design requirements for FTS, though there are already successful lab-scale and pilot-scale FTS microchannel reactors (see Table 5), and a clear catalogue of design strategies has not yet been published. A selection of review papers related to microreactor design are summarized in **Table 1** and show investigation trends in catalyst development and reaction mechanism, reactor design and fabrication, operation, and process simulation. However, though the heat transfer in microreactors is recognized as a major design aspect and has been extensively reported, the interrelated effects of dimension-, material- and operation parameters have not been studied for specific reactions. Furthermore, transferring design experiences from heat sink or other catalytic reactions to the FTS process is seldom discussed.

Table 1. Summary of recently published reviews related to microreactor design. (+) indicates a positive contribution to knowledge and (-) indicates a knowledge gap.

Refs.	Main topics	Contributions and knowledge gaps regarding reactor design
2018 Naqiuddin, et al.[25]	1) Micro heat sink with straight/wavy/pin-fin/ribs/dimples/oblique fin channels and coolant 2) Numerical simulation of heat removal and fluid flow distribution 3) Application in electronics systems, solar cell, fuel cell, and medical devices	(+) Design of heat sink was summarized. (−) Design transfer to heat management for catalytic reaction systems is not scoped.
2018 Suryawanshi, et al.[26]	1) Materials for microreactor fabrication, fabrication methods 2) Microreactor application in the field of nanoparticles, polymers, organic chemicals and medicines	(+) Microreactor fabrication was summarized. (−) Microreactor design is not included.
2020 Engelbrecht, et al.[27]	1) Autothermal operation with exothermic and endothermic reactions 2) Heat exchange configurations of counter-current flow/co-current flow and cross flow	(+) Autothermal reaction systems with heat exchange configurations of counter-current flow/co-current flow and cross flow were summarized. (+) A variety of design aspects are discussed including wall materials, channel dimensions, catalyst positioning, feed gas distribution, heat recirculative reactor geometry, manufacturing tolerance, catalyst sintering, pressure drop, shape of channel, coating methods, and deactivation. (−) Design transfer to the FTS process or other catalytic reactions is not discussed.
2020 He, et al.[28]	1) Catalytic methane combustion (CMC): catalyst, reaction mechanisms, and conditions 2) Applied reactors: fixed-bed reactor, wash-coated reactor, membrane bed, fluidized bed	(+) Catalyst types and forms, reactors including microchannel type, and effects of operational factors for CMC were surveyed. (−) Effects of heat management, mass transfer, fluid dynamics on microreactor design are not scoped. (−) Design transfer from CMC to FTS process or other catalytic reactions is not considered.
2021 Dong, et al.[29]	1) Numbering up and sizing up strategies of the micro- and milli-reactors 2) Scaling factors based on dimensionless numbers	(+) Numbering up: design experience for even flow distribution was summarized. (+) Sizing up: theoretical scaling factors of residence time distribution, mixing performance, heat transfer, and mass transfer were discussed. (−) Parameterization for distinct catalytic reactions is not considered.
2022 Harris, et al.[30]	1) Heat transfer and thermal management in the microchannel reactors	(+) Summarized effects of materials (working fluids, nanofluids/nanoparticles, and surface treatment/manipulation), experimental elements (flow boiling, phase change, flow resistance, thermal resistance, and manufacturing techniques), and design (aspect ratios, geometry/shape manipulation, barriers, and pin-fins). (−) Design principles for FTS process and the feasibility of parameterization for other catalytic reactions are not discussed.
2022 Teimouri, et al.[31]	1) Computational fluid dynamics for FTS 2) Slurry bubble column reactors, fixed-bed reactors, circulating fluidized beds, membrane reactors, and microchannel reactors 3) Empirical and semi-empirical kinetic models	(+) Simulation experience (kinetic models, parameterization, etc.) for FTS microreactor was presented. (−) Design principles for FTS process are not scoped.
2024 Apolinar-Hernández, et al.[18]	1) Market, material, reactor, process, and reaction mechanism for low-temperature FTS	(+) General introduction of advantages and challenges for fixed bed reactors, slurry reactors, and microreactors. (−) Design principles for FTS process are not scoped.
2024 Yadav, et al.[32]	1) Autothermal conditions achieved in microreactor for steam reforming 2) Considerations for numerical models 3) Effects of microchannel design, catalyst and operation conditions on steam reforming performance based on numerical findings	(+) Trends analysis on the effects of microchannel structure, aspect ratio, shape, dimension, manifolds, catalysts, operation conditions and materials on flow and temperature distribution based on numerical examples for endothermal reaction were presented. (−) Engineering design strategies are not discussed. (−) Design transfer to the FTS process or other catalytic reactions is not discussed.
2025 Ganjkhanlou, et al.[17]	1) Low-temperature FTS using microreactor for biosyngas conversion 2) Structure, shape, materials of microreactor, catalyst and loading, cooling methods for effective heat dissipation	(+) Existing experiences of heat management for low-temperature FTS were mainly focused. (−) Effects of mass transfer, fluid dynamics on microreactor design are not scoped.

(*Continued*)

Table 1. (Continued)

Refs.	Main topics	Contributions and knowledge gaps regarding reactor design
Current review	1) Summary of design strategies for FTS microreactors 2) Considers various reactor types e.g., packed bed and the wash-coated under forms of microchannel and microtube, micro-monolith, and micro-structured reactor	(+) FTS microreactor design strategies considering heat transfer, mass transfer, flow field and pressure drop, and residence time distribution for cross section, channel geometry/arrangement, reactor materials, catalyst dimension, microstructure, operation conditions. (+) Design extension for other catalytic processes is discussed. (−) Detailed design methodologies are excluded from the scope.

Thus, there is an immediate need for a comprehensive design strategy for the FTS process.

Motivated by the current knowledge gap regarding microreactor design for FTS, this review starts with a summary of design strategies for the FTS process considering heat transfer, mass transfer, pressure drop, residence- and contact time. Dimension- (cross section, channel geometry, channels arrangement, volumetric/surface structure, particle size/catalyst thickness, microstructure), material- (reactor materials, catalytic support material), and operation-related (catalyst loading method, pressure drop, residence time distribution) parameters are summarized, and scaling-up strategies are also discussed. Later, the design extension from FTS to other catalytic reactions is theoretically discussed. Limitations in experiments and simulations in the literature and challenges will be noted, and future directions for investigations of microreactor design are suggested. It is noted that, though the detailed design methodologies are excluded in the current review, it is our hope that this review might serve as an engineering guide for the design of catalytic microreactors and spur more detailed research into design parameters and different catalytic applications. For the sake of space, topics related to microreactors such as detailed catalyst mechanisms, catalyst preparation, operation schemes, economic constraints, and strict safety constraints are also excluded in this review.

2. Fischer–Tropsch synthesis in Microreactors

Microreactors are distinguished from industrial/large-scale FB, SB, and CFB reactors in several features:

Heat transfer in microreactors by thermal conduction is more dominant than by convection due to the laminar flow pattern (as elaborated in the following sections). Also, due to the short heat transfer lengths inside the channels, the cross-sectional temperature distribution of microreactors is almost homogeneous. Temperature gradients mainly exist along the flow direction as the reaction progresses along the reactor (e.g., temperature increase due to the exothermic reaction of FTS process). However, with a combination of small dimensions and optimized heat exchange design (i.e., active thermal management as elaborated in the following sections), microreactors can potentially achieve isothermal conditions across the whole reactor. Thus, all the catalysts in the microreactor can run at an optimal temperature, thus maximizing the utilization of catalysts, maximizing production, enabling higher control of product selectivity, and enhancing catalyst stability.

Moreover, microreactors also have advantages of short diffusion lengths of reactants and products to and from the catalyst active sites, mitigating mass transfer limitations and allowing the catalysts to potentially operate at peak efficiency.[33] Additionally, the typical flow pattern in microreactors is laminar, such that fluids follow along smooth paths in layers, with each layer passing by the adjacent layers with little or no mixing. Instead, radial mixing is dominated by diffusion. Thus, increasing the mixing efficiency while preserving a relatively low pressure drop in a microreactor can be challenging for the design. Further, due to the absence of dead volumes and overall small dimensions, the RTD in the microreactor is quite narrow with $Pé > 10^2$ (see following sections) compared to the large-scale reactors (e.g., slurry bed reactor: $Pé < 10^{-2}$–10^0).[34,35] Ensuring a narrow RTD can minimize unwanted subsequent reactions while sustaining sufficient reaction time for high conversion to the desired products.

Those features of heat-, mass transfer, and fluid dynamics characteristics of a reactor can be described by various dimensionless groups, which are also often used as scaling factors[29] as well as the key criterion for comparison of different reactor setups. The dimensionless groups commonly used for microreactors include the Reynolds number, the Nusselt number, the Biot number, the Sherwood number, the Schmidt number, the Bodenstein number, the Péclet number and the Damköhler number. The range of these dimensionless numbers, definitions of Mears criterion and Thiele modulus, equations for pressure drop and mean residence time are introduced and given in Section 2.1; design parameters (e.g., hydraulic diameter d_h) related to those dimensionless numbers for heat transfer, mass transfer, pressure drop and residence/contact time and distribution for mainly FTS are summarized and discussed in Sections 2.2 and 2.3. Based on the summary, design boundaries for FTS microreactors are underlined, and overall design comparison among different catalytic reactions is presented in Section 2.4.

2.1. Theoretical Background

Reynolds number, *Re*, is the first basic dimensionless number for descriptions of heat transfer, mass transfer, and flow hydrodynamics in reactors, with:

$$Re = \frac{\rho_f u_f d_h}{\mu_f} \tag{5}$$

where ρ_f and μ_f are the density [kg·m^{-3}] and viscosity [Pa·s] of the fluid, u_f is the flow velocity [m·s^{-1}] and d_h is the hydraulic diameter [m] (see Equation (4)). *Re* describes the ratio between inertial and viscous forces and is affected by fluid temperature, velocity, and microreactor size. *Re* ranges commonly from 10^0 to 10^2, indicating a laminar flow pattern,[36] whereas *Re* for large-scale reactors (e.g., CFB) is much larger than 2000 in order to

cause flow turbulence. Design of microstructure and/or roughness could, however, lead to a change of transition between laminar and turbulence,[37] due to the occurrence of secondary flows or local vortices in the microreactor. Related to FTS process, the existence of liquid film may cause large disturbance waves at $Re > 400$ inside vertical tubes.[38]

The Nusselt number, *Nu*, and Biot number, *Bi*, are usually used to describe the heat transfer phenomena in the fluid as well as in the adjacent solids (i.e., reactor wall, catalyst, and/or catalytic support), with:

$$Nu = \frac{h_f d_h}{\lambda_f} \tag{6}$$

$$Bi = \frac{h_f d_h}{\lambda_w} \tag{7}$$

where h_f is the convective heat transfer coefficient [$W \cdot m^{-2} \cdot K^{-1}$] in the fluid; λ_f and λ_w are the thermal conductivities of the fluid and solid wall [$W \cdot m^{-1} \cdot K^{-1}$], respectively. As seen from Equations (6) and (7), *Nu* is the ratio of convective to conductive heat transfer at the boundary in a fluid while *Bi* is the ratio of the thermal resistance for conduction inside the solids to the resistance for convection at the surface of the solids. Due to the strong correlation to *Re* number and micro dimension of the reactor, both numbers are in the range of 10^0–10^1. By increasing secondary flows or vortices in the laminar flow field, *Nu* increases; with increasing λ_w, reduces *Bi*, i.e., the temperature distribution in the solids is more uniform than that in the fluid. To achieve isothermal conditions, careful design of reactors, catalysts, operational conditions, etc., should lead to large *Nu* and small *Bi*.

Mass transfer is commonly described by the Sherwood number, *Sh*, the Schmidt number, *Sc*, as well as the Bodenstein number, *Bo*, or Péclet number, and is estimated by Mears criterion and Thiele modulus.

Sh characterizes the ratio of total mass transfer rate from convection and diffusion to the rate of diffusive mass transport and has a strong correlation to *Re* and *Sc*:

$$Sh = \frac{h_m}{\frac{D_e}{d_h}} \tag{8}$$

where h_m represents the total mass transfer rate [$m \cdot s^{-1}$] and D_e represents the effective diffusivity [$m^2 \cdot s^{-1}$]. *Sh* is also known as the mass-transfer Nusselt number, while some researchers refer to it as the Biot number for mass transfer, Bi_m.[39] The *Sc* number physically describes the ratio of relative thickness of the hydrodynamic layer and mass-transfer boundary layer:

$$Sc = \frac{\mu_f}{\rho_f D_e} \tag{9}$$

Though it is widely believed that mass transfer resistances are negligibly small in a microreactor, modelling considerations for *Sh* and *Sc* and effective diffusivity D_e are quite complex. It is noteworthy that due to its laminar flow pattern the difference in gas diffusivities and/or solubilities (i.e., H_2 and CO for FT process) may have a large impact on catalyst performance in the microreactor. For example, one simulation study showed that mass transfer diffusion resistances strongly affect the selectivity and activity of catalysts.[39] Owing to the fact that the accessibility of all reactants upon catalyst active sites is different, and thus, it could result in performance deviation from the ideal reactor model, where mass transfer limitation is not considered, and all gas species are equally transported to the catalyst.

Apart from diffusion on a micro scale, the reactants and products experience lateral and axial dispersion in the reactor on a macro scale. The Bodenstein number (*Bo*, sometimes also referred as Péclet number, $Bo = Pé\ L/d_h$) describes the axial dispersion and thus the extent of back-mixing in a reactor.[40] In Equation (10), D_{ax} is the effective axial dispersion-diffusion coefficient [$m^2 \cdot s^{-1}$], which comprises all effects of back-mixing, e.g., radial velocity profile in laminar flow, molecular diffusion, eddies, and vortices.

$$Bo = \frac{u_f d_h}{D_{ax}} \tag{10}$$

According to Equation (10), a small *Bo* indicates a large axial dispersion and diffusion, and correspondingly, a broad RTD. The common threshold for an assumption of "ideal plug flow reactor (PFR)" for the microreactors is $Bo \geq 10^2$,[29,41,42] and *Bo* number drops dramatically in larger reactors. In principle, PFRs with a narrow RTD are usually desirable. To reduce the axial dispersion, microstructures are introduced in the reactor, generating chaotic secondary flows that enhance radial mixing and thus disturb the laminar flow profile. However, the microstructure of the catalyst/reactor surface/catalytic support should also be carefully designed to avoid large external mass transfer resistance. For this, the Mears criterion[43] is typically used to estimate the external mass transfer resistance of a catalyst. Mears number *M* is the mass transfer rate relative to the intrinsic rate with no transport limitations around the catalyst. External mass transfer resistance is negligible if the following relationship holds:

$$M = \frac{-r \rho_{cat.} d_p n}{kC} < 0.15 \tag{11}$$

where *r* is the reaction rate [$kmol \cdot kg_{cat}^{-1} \cdot s^{-1}$], $\rho_{cat.}$ is the bulk density of the catalyst [$kg \cdot m^{-3}$], d_p is the radius of the catalyst particle [m], *n* is the reaction order, *k* is the mass transfer coefficient [$m \cdot s^{-1}$], and *C* is the bulk concentration of the reactant [$mol \cdot m^{-3}$].

On the other hand, the dimensionless Thiele modulus Φ_n is often used to estimate internal diffusion limitations within a catalyst.[44,45] As shown in Equation (12), the Thiele modulus is the square root of the ratio of the surface reaction rate to the rate of diffusion through the catalyst. Large Φ_n indicates that internal diffusion limits the rate of the reaction, and typically, Φ_n less than 1 suggests negligible internal diffusion limitation of the catalyst.

$$\phi_n = L\sqrt{\frac{\rho_{cat.}(-r)}{D_e C}} \tag{12}$$

The Damköhler number (*Da*) is also extensively applied for reactor design, and it relates the chemical reaction rate to the mass transport rate in a reactor, such as volumetric flow rate.

$$Da = \frac{\text{reaction rate}}{\text{mass transport rate}} \tag{13}$$

Generally, the lateral *Da* number (or second *Da* number, which designs the cross section of a reactor) is smaller than 10^{-1}, so that the cross-sectional concentration gradient is relatively small for the microreactors. Due to the small dimension of microreactors (with d_h of 10^{-2}–10^{1} [mm]) as well as the high gas diffusivity $Da \leq 10^{-1}$ is not difficult to achieve. Conversely, for large-scale reactors a small concentration gradient is difficult to maintain, since catalyst activity does not increase linearly with the reactor dimension. Thus, increasing mass transport rate via flow turbulence to minimize mass transfer resistance is often aimed during the design of large-scale reactors, e.g., SB and CFB, yet, this may also lead to an enormous rise in pressure drop, e.g., in FB. On the other hand, the lengthwise *Da* number (or first *Da* number, which designs the length of a reactor or catalyst bed) is usually $\geq 10^{0}$–10^{1}, thus the reactants have sufficient residence/contact time in the reactor.[34,46,47] This criterion for both large- and small-scale reactors should be maintained, however, for slurry bed reactors, $\geq 10^{1}$–10^{2} may be needed due to their large degree of back-mixing.

Pressure drop is an integral observation of fluid dynamics in the reactor. The Ergun equation[48] is often used to describe the pressure drop in packed-bed reactors for both large- and small-scale reactors:

$$\frac{\Delta P}{L_{cat.}} = E_1 \frac{(1-\varepsilon)^2}{\varepsilon^3} \frac{\mu_f u_f}{{d_p}^2} + E_2 \frac{(1-\varepsilon)}{\varepsilon^3} \frac{\rho_f {u_f}^2}{d_p} \tag{14}$$

where E_1 and E_2 are viscous and kinetic constants, respectively; ϵ and $L_{cat.}$ are the porosity (or holdup) of the catalyst bed and the length of the catalyst bed, respectively. Nevertheless, the Ergun equation was found to be valid only for narrow size distributions of particles, spherical particles, and fails to predict pressure drops when wall-channeling effects (since the near wall velocity of the fluid differs from that at the center of the packed bed) are strong.[49] Therefore, separately, the pressure drop for a wash-coated channel is usually derived from the Bernoulli equation:[50]

$$\frac{\Delta P}{L_{m.r.}} = \frac{C'}{Re^n} \cdot \frac{\rho_f}{2 d_h} {u_f}^2 \tag{15}$$

where C' and n depend on the flow conditions and channel geometry, C'/Re^n is a friction factor, $L_{m.r.}$ is the reactor length. It should be noted also, when catalyst dimension is within the same magnitude of reactor dimension, i.e., $d_p \sim d_h$, pressure drop should be calculated by Equation (15).

Residence time indicates hydrodynamic residence time, which describes the time duration that the reactant molecules/atoms spend in the gas/liquid phase of the reactor (or control volume), and residence time distribution (RTD) is usually applied to describe a reactor without involving reaction. The mean residence time (τ, s) of RTD is calculated as:

$$\tau = \frac{V}{\upsilon} \tag{16}$$

where V is the free vessel volume [m^3] (no dead volume in the reactor) and υ is volumetric flow rate [$m^3 \cdot s^{-1}$].

Dimensionless numbers, as compared in **Table 2**, though a few of them apply similarly for both large- and small-scale reactors, indicate that the phenomena of heat-, mass transfer, and hydrodynamics in microreactors are quite different from large-scale reactors, and thus the design principle should also be applied differently. Detailed design parameters related to those dimensionless numbers for microreactors, e.g., cross section, channel geometry, channels arrangement, volumetric/surface structure, particle size/catalyst thickness, microstructure, reactor materials, catalytic support material, catalyst loading method, pressure drop, residence time distribution, will be focused and summarized and their role in the design of FTS microreactors discussed in the following sections.

2.2. Categories of Microreactors

Before diving into the summary of design strategies for microreactor, the definitions and classifications should be clarified. The definitions of "micro-" for the microreactors in the literature are scattered, e.g., a channel with width in the magnitude of 10^2 mm is notified as microchannel in some works.[51] Currently, in the present literature, terms such as "microchannel", "microstructured", "micro-monoliths" are often used to describe different reactors, but an inconsistency of the assignment prevails. For clarity in this review, the term microreactor is collectively used to describe various "micro" reactors with d_h of 10^{-2}–10^{1} [mm] which are further categorized into microchannels, microtubes, micro-monoliths, and micro-structured reactors, as illustrated in **Figure 2**.

The cross sections of the microchannels are often rectangular and the aspect ratio (i.e., $\alpha = \frac{W_{m.r.}}{H_{m.r.}}$, the ratio of width to height of the channel) ranges from 10^0 to 10^1,[30] which means the height of the microchannel is usually the smallest dimension. Other designs, e.g., trapezoidal- and triangular cross sections, are also categorized as microchannels in this review.[52] The characteristic dimensional parameters are height, width, length, and/or hydraulic diameter. The flow path of the reactant and product is usually straight, however, zigzag-,[53,54] sinusoidal-[55,56] and other complex[57] designs also exist.

The cross-section of a microtube is either circular or annular.[4] The characteristic dimensional parameters are the inner diameter (i.d.) and/or annular gap distance. The main distinguishment between microchannel and microtube is the corner effects: the cross-sectional Sherwood number *Sh* at $Pé < 1$ as well as friction factor C'/Re^n (refer to Equation (15)) for circular shape are larger than for the shapes with corners.[58–60] Both multi-microchannel or -tube reactors often consist of parallel arranged microchannels or -tubes and all units are assumed to have identical performance.

The scale of the monolith body is 10^1–10^2 [mm], but the cross-section of the channels in the monolith is 10^{-1}–10^1 [mm], as seen

Table 2. Summary of dimensionless numbers between microreactor and conventional reactors for FTS process. ↑ indicates increase of effects or values, ↓ indicates decrease of effects or values.

	Microreactors							Conventional reactor
	Cross section $d_h \approx 10^{-2}$–10^{1} [mm]	Length $L \approx 10^{2}$ [mm]	Microstructure $H_{m.st.}/H_{m.r.} > 10^{-1}$	Material thickness 1×10^{-3} [m]	Catalyst	Scale up-numbering up	Liquid formation	(slurry bed)
Re	10^{0}–10^{2}				packed-bed: <1.5 [bar·m^{-1}] wash-coated: ≈10^{-3} [bar·m^{-1}]		*Re* ↑, liquid drainage ↑	> 10^{3} [a]
Nu	10^{0}–10^{1}	lengthwise ΔT ≤0.002 [°C·mm^{-1}]	secondary flows ↑, *Nu* ↑		packed-bed: d_h with upper limit wash-coated: d_h with lower limit			10^{2}–10^{3} [a][130]
Bi				10^{0}–10^{1} λ of wall and support ↑, *Bi* ↓				10^{0}–10^{1}
Sh	2-phase gas-solid system: 10^{0}–10^{1}[60]		structure packing: *Sh* ↑ BET> 10^{3} [m^{2}·g^{-1}], *Sh* ↓		particle size: 80–100 [µm] layer thickness: ≤100 [µm]		liquid drainage ↑, *Sh* ↑	>10^{1}[60]
Sc	Gas phase: 10^{-1}	straight geometry: liquid drainage ↑					Liquid formed: 10^{4}	Liquid: 10^{4}
Bo	α (<0.5, >3): *Bo* ↑		secondary flows ↑, *Bo* ↑			sizing up: *Bo* ↓↓	α (0.5–3): *Bo* ≥10^{2}, channel blockage ↓	<10^{-2} [a]
Da_I [b]		≥10^{0}–10^{1}						≥10^{1}–10^{2}
Da_{II} [c]	≤10^{-1}				catalyst loading: packed-bed > wash-coated	sizing up: Da_{II} ↑↑		≤10^{-1}

[a] High degree of convection, associated with turbulence [b] Lengthwise *Da* number or first *Da* number [c] Lateral *Da* number or second *Da* number

in Figure 2c. Some researchers also refer to micro-monolithic reactors as micro-structured reactors.[5] The commonest cross-sectional geometry of monolith channel is square, but round and triangular designs also exist.[28,61] The characteristic dimensional parameters are the hydraulic diameter of the channel and the cell density (i.e., cells per square inch, cpsi). The cell density of micro-monoliths ranges from 1200 to 200 cpsi, corresponding to a hydraulic diameter of 0.3 to 0.8 [mm], implying that the greater the cell density, the smaller the monolithic channel.

Microstructures in a mm- or cm-scale reactor (usually cut as cylinder shape) refer to the 3D random or periodic structures, where straight flowing paths do not exist, and the reactant and products are forced to change their flow direction according to the microstructures. Typical examples of microstructures in the literature are foams[62,63] and cross flow structures (including open cross flow structure, OCFS, and closed cross-flow structures, CCFS, see **Figure 3**).[64,65] The characteristic dimensional parameters are the hydraulic diameter of the micro "pore" and the pore density (pores per square inch, ppsi). The pore density of the foam structure is around 50 ppsi, corresponding to pore hydraulic diameters ranging over 0.3–0.8 [mm]. Other examples of random 3D microstructures are presented in Figure 3a–d, and these can be grouped into those with surface-wise 3D microstructure (in Figure 3a,b), and volume-wise ones (c and d).

Unlike microchannels and microtubes, where the cooling channels can be located next to the microreactors, no cooling is conducted within the micromonolith and microstructures (reactor cross-sectional dimension could be $> 10^2$ [mm]), though the channel walls can serve as a guide for the flows of heat transfer media.[61,71] Therefore, the heat transfer properties between microchannel/microtube and micromonolith/microstructures can be very different and should be well considered during reactor design.

Catalyst loading methods in different microreactors (see Figure 2) can be further sorted into packed-bed and wash-coated, as presented in **Figure 4**.

In a packed bed, the catalyst is randomly packed in the microreactor. Though packed bed loading is widely used, it suffers from various shortcomings: severely limited inter- and intra-particle mass and heat transfer, thus hot spot formation, high pressure drop, and poor drainage of, especially, FT liquid products. The main reason is that its high ratio of volume to wall area can result in less effective heat removal. Instead of random particle packing, structured packings via microstructures (see Figure 2c,d) have been proposed to increase heat transfer and decrease the pressure drop, consequently enabling the packing of smaller catalyst particles, reducing the intra-particle mass transfer.[62,64] Examples of packing structures (e.g., monolith, OCFS, and CCFS) are given in Figure 3.

For wash-coating, the catalyst is loaded in the reactor by applying stable slurries of the catalyst with small particle sizes, i.e., $\approx 10^0$–10^1 [μm], to the reactor walls, then fixing them by calcination. Since the catalyst is directly loaded onto the reactor walls, efficient heat removal can be realized and the flow in the reactor has a laminar profile. Wash-coated microreactors own intrinsic advantage on lowing pressure drop in magnitude of 10^{-3} [bar·m^{-1}][61] and thus intensify catalyst utilization[61] as well as heat transfer,[72] though the total catalyst loading is much lower than packed-bed ones. However, increasing catalyst thickness could trigger large mass transfer resistance and further affect the catalyst performance.[63,73]

Owing to the fact that the vast majority of microreactors studied in the literature are of the microchannel type, and thus, the summary in the following sections focuses more on this type. However, where cited experimental investigations and simulation models use other types of microreactors, this is mentioned.

2.3. Design Strategies

An overall schematic of design strategies in this section is presented in **Figure 5**. We summarize and discuss reports on the findings of the key criteria under each design item (i.e., heat transfer, mass transfer, pressure drop, and residence/contact time and distribution) for mainly FTS. However, as seen in Figure 5, some parameters, e.g., dimension and geometry of reactor and of microstructures, for individual design items may overlap with other items, which means that the design of these parameters should reconcile the conflicting requirements of several aspects. Therefore, the related design parameters will first be separately discussed in each section and their design boundaries be summarized in the last section. We close by a preliminary comparison for design transfer from FTS to other syngas-related processes from the engineering perspective as well as examples of existing scaled-up set-ups.

2.3.1. Heat Transfer

Reactor design with prudent considerations on heat transfer is imperative to avoid the formation of hot spots and/or thermal run away, and furthermore, to intensify the production and to allow drainage of waxy products. To address this, the following design

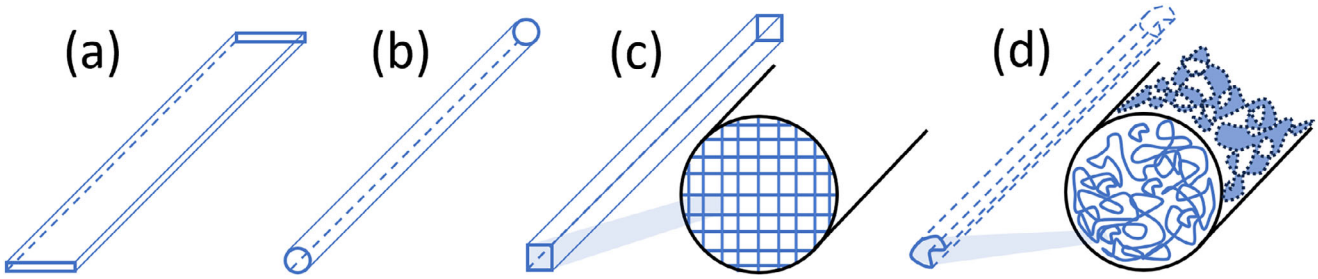

Figure 2. Types of microreactors: a) microchannel; b) microtube; c) micro-monolith; d) micro-structured reactor.

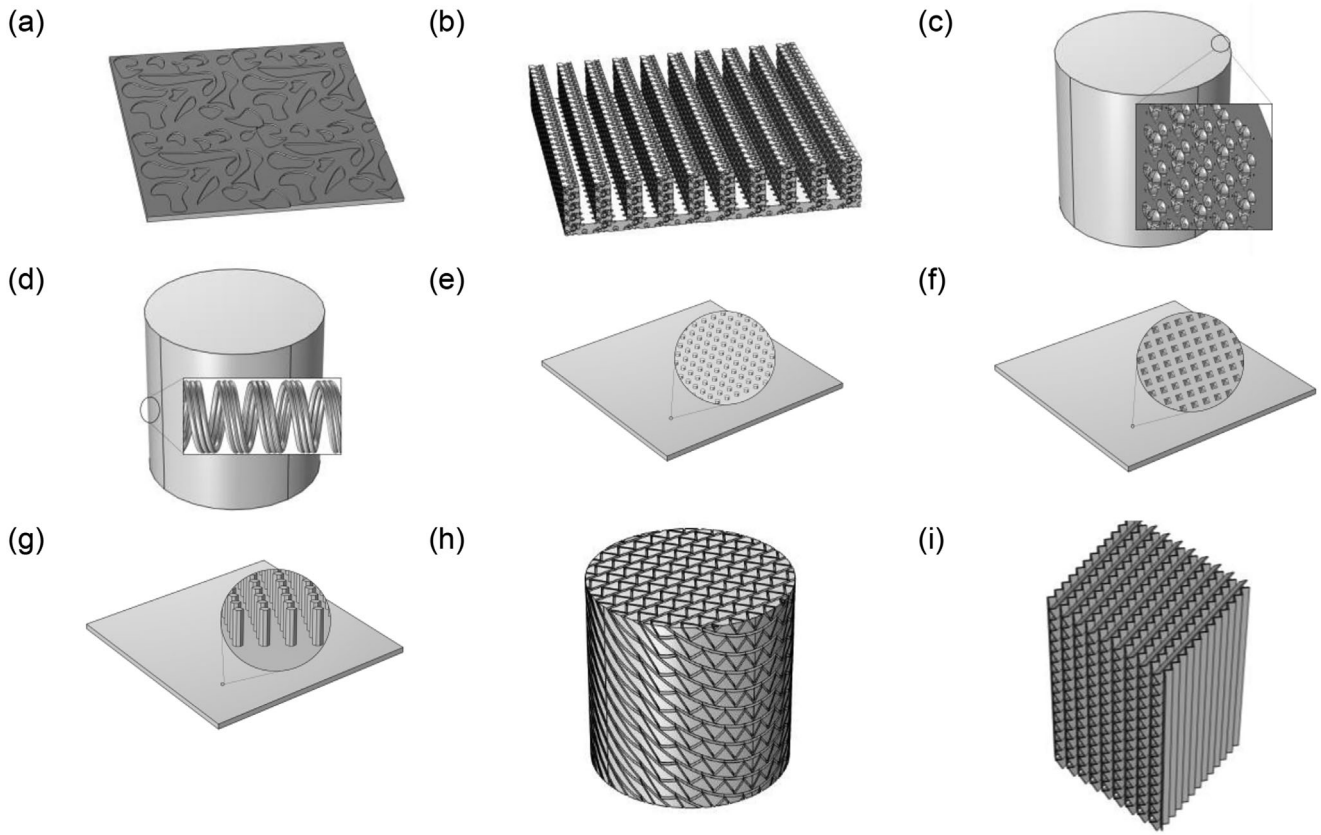

Figure 3. Examples of 3D microstructure. a) Surface-wise micro-structured plate (e.g. etched stainless steel in ref. [66]); b) Foam microchannel plate (e.g. metal foam microchannel in ref. [66]); c) Volume-wise micro-structured packing (e.g. aluminum-foam packing in ref. [67]); d) Volume-wise micro-structured packing (e.g. knitted wire packing in ref. [68]); e) Surface-wise micro-structured-pillar plate (e.g. microstructured foils in ref. [19]); f) Surface-wise micro-structured-pyramid plate (e.g. microstructures on thin film in ref. [69]); g) Surface-wise micro-structured-pillar plate (e.g. silicon-pillar microstructure in ref. [70]); h) CCFS packing element (e.g. in ref. [64]); and i) OCFS packing element.

aspects must be considered, including cross section, channel geometry and arrangement, microstructure, as well as the selection of materials of the reactor wall and the catalyst support.

Cross Section: Two aspects need to be considered in terms of "cross section" design of the microchannel reactors namely, the geometry and the dimension.

With respect to geometry, the majority of the microchannels are designed with a rectangular cross section, though some are circular, trapezoidal or triangular. Each design may present a different temperature profile distribution. Based on the 3D simulation, Ramanathan et al.[74] suggested that sharp corners have high local *Da* number, which leads to uneven temperature distri-

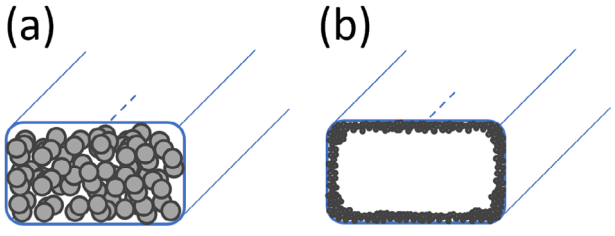

Figure 4. Catalyst loading methods showing a) packed-bed and b) wash-coated microchannel.

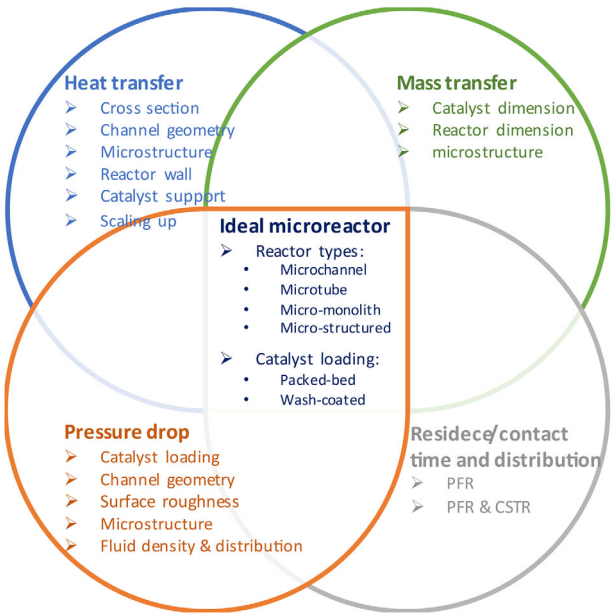

Figure 5. Schematic of design strategies.

bution across the cross section, while circular and hexagon geometry could cause a lower average wall temperature. On the other hand, simulation results by Gunnasegaran et al.,[52] comparing the heat transfer among rectangular, trapezoidal and triangular microchannel reactors with parallel arrangement, indicated that the rectangular geometry has a higher heat transfer coefficient at the same Reynolds number. It is mainly because rectangular geometries can facilitate large contact areas between microchannels and cooling channels (i.e., top and base surfaces, relating to width W), while minimizing heat exchange with other parallel microchannels (i.e., side surfaces, relating to height H, and $W \geq H$), compared to trapezoidal and triangular geometries.

Dimensions are typically described by the height/diameter of the section and/or the aspect ratio. The height ($H_{m.r.}$) of the rectangular cross section is commonly in the range of 0.5–2 [mm],[13,14,51,55,75–78] although some smaller ($H_{m.r.}$ = 0.1–0.25 [mm])[52,56,57,79–83] and some larger ($H_{m.r.}$ = 3–8 [mm])[14,84,85] have also been reported. Typically, the aspect ratios ($\alpha = \frac{W_{m.r.}}{H_{m.r.}}$) of microchannel reactors are in the range of 0.5–3. Experiments and simulation results show that the cross-sectional temperature difference in rectangular 10 [mm] × 5 [mm] ($W_{m.r.} \times H_{m.r.}$) FTS microchannels can be within 3 [°C] or 0.06 [°C·mm^{-2}].[84] And it is generally believed that the smaller the cross-section, the smaller the temperature difference, thus, cross-sectional temperature difference is seldom reported and microchannel reactors with cross-section d_h 10^{-2}–10^{1} [mm] is mostly treated as 1D reactor (see Table 6), i.e., isothermal condition in the radial direction.

In short, for small cross-sectional temperature/concentration gradients, sharp corners should be avoided; for better heat removal, when using cooling channels, a rectangular geometry is more ideal and practical. Considering the trade-off between cross-sectional temperature distribution and heat transfer capacity, rectangular geometry with α = 0.5–3 and $H_{m.r.} \leq 5$ [mm] seems to be appropriate in microchannel reactors.

Length: Possible large temperature gradient exists in axial direction of the microreactors compared to radial direction, as the FT reaction continues and different CO conversion level as well as product selectivity, thus different reaction heat release, exist along reactor length. Longer reactors have a larger heat exchange surface, nevertheless, it should be noted that the total length of microreactors may in some cases be longer than the length of the walls in contact with the catalyst, $L_{m.r.} \leq L_{cat}$. Mostly, when the catalyst is loaded directly on the reactor walls by wash-coating, $L_{m.r.} = L_{cat}$.[51,53,55,75–77,79,80] However, when the catalyst is packed in reactor volume or is wash-coated onto a microstructure which is inserted in the reactor, (0.5–1.0)$L_{m.r.} = L_{cat}$.[10,13,65,71,84,86–88] To reduce complexity, this review addresses effects related to the length on which the catalyst is applied in the reactor.

For sufficient heat transfer and efficient reaction, the length of the microreactor should be designed according to the amount of heat removed as well as the residence time needed for chemical reaction.[89] The lengths of FTS microreactors reported in the literature on investigations of heat transfer, range from 50 to 600 [mm], including microchannel reactors and other types,[13,14,52,57,74,76,77,81–83,88] and they seem to claim to be free from thermal runaway. Deshmukh et al. experimentally compared four different microchannel reactors (length of reactor: 70–635 [mm], length of catalyst: 38–619 [mm], hydraulic diameters of cross section: 1.4–1.8 [mm]) for FTS.[13] They found that at typical FTS conditions, the catalyst contact time of 209–355 [ms], corresponding to space velocities of 10 000–17 000 [h^{-1}], yields CO conversions of 60–70%, with a CH_4 selectivity of 7–10% and a C_{5+} selectivity of 80–87%, while the temperature difference along the reactor length was kept below 2 [°C] regardless of whether the reactor length was 70 [mm] or 635 [mm]. They thus concluded that in their case, the channel length does not affect the catalyst performance. Indeed, by changing operating conditions, e.g., space velocity, as also in their experiments, to achieve nearly isothermal condition, different microchannel dimensions can perform similarly. However, the length of microchannel should be constrained due to the temperature rise as well as heat evolution which results from the change of CO conversion along the length. Thus, based on reported reactor design, it seems practically feasible to control small temperature gradients by applying reactor lengths within magnitude of 10^2 [mm], which, of course, might vary due to operation conditions and applied microstructures (e.g., temperature difference around 0.002 [°C·mm^{-1}] along length of a packed-bed FTS reactor is reduced to around 0.001 [°C·mm^{-1}] due to the CCFS packing structure in the reactor, based on one simulation study [64]).

Although most channel geometry designs are straight, other designs, e.g., zigzag,[53] sinusoidal[55,56] and complex[57] shapes, are proposed to enhance flow turbulence and heat transfer. The main idea is to bring parts of the channel with different temperatures together, shorten distance for heat transfer and simultaneously create flow turbulence. However, such geometric effects on *Nu* number/heat transfer coefficient are limited,[55] since the flow pattern in the microreactor is usually laminar. For the FTS process, complex-geometry channels are seldom mainly because of the difficulty of the liquid-product drainage. Therefore, straight channels are preferred, which is also favorable from the manufacturing point of view.

Microstructure: Examples of 3D microstructures (i.e., random- and controllable structures) are shown in Figure 3 and they can be applied as catalyst supports, reactor surface or structuring packing. The ratio of the height of the microstructures or roughness element and the height of the channel (i.e., $H_{m.st.}/H_{m.r.}$, illustrated in **Figure 6**) is applied in this review. Simulation results from Zhai et al. ($H_{m.st.}/H_{m.r.}$ = 200 [μm]/400 [μm]),[57] Dharaiya et al. ($H_{m.st.}/H_{m.r.}$ = 50 [μm]/400 [μm]),[83] Foong et al. ($H_{m.st.}/H_{m.r.}$ = 134 [μm]/200 [μm])[81] and Copiello and Fabbri ($H_{m.st.}/H_{m.r.}$ = 0.75)[90] concluded that microstructures (as roughness elements) could enhance the heat transfer of the microreactors. It is mainly because that microstructures of $H_{m.st.}/H_{m.r.} > 10^{-1}$ could cause flow-profile changes and even early occurrence of the turbulence.[37] Two studies on microstructured reactors with powder catalyst packed between micropillars ($H_{m.st.}/H_{m.r.}$ = 400–750 [μm]/800–1200 [μm], illustrated as Figure 3f,g were tested under FTS conditions, found that the chain growth probability was affected by the width of the reactor slit with only a slight temperature gradient.[19,91] However, no benchmark experiments were done to compare the effects of the micropillars on the FTS performance as well as temperature distribution. Nevertheless, it can be concluded from the current experience that a surface roughness of $H_{m.st.}/H_{m.r.}$

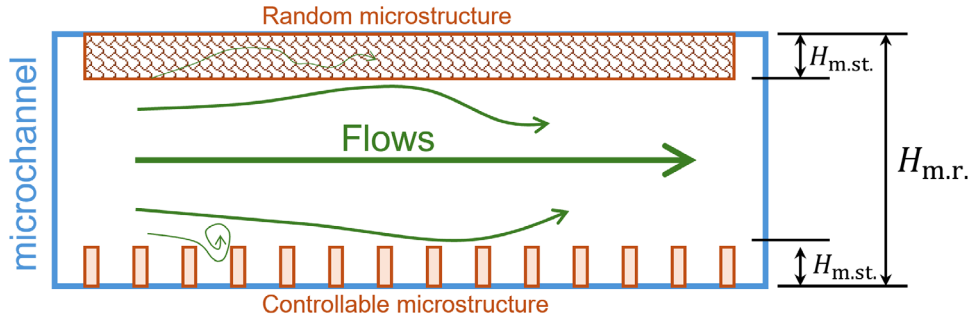

Figure 6. Schematic of a microchannel depicting height of the channel and the height of microstructures or roughness.

= 0.35–0.75 could cause changes in the flow profiles, which to some extent enhance heat transfer, without significantly increasing the pressure drop.

Furthermore, 3D microstructures such as micromonoliths in the reactor can serve as catalytic support and heat transfer media. A set of simulations for OCFS and CCFS structures in FTS packed-bed reactors were carried out.[64,65] The results indicated that the packing structures increase the uniformity of the temperature distribution along reactor length and decrease the pressure drop compared to randomly packed bed. Thus, they suggested the particle size for the packed bed with OCFS and CCFS structures can be smaller compared with the randomly packed bed, which can increase catalyst loading and catalyst contact surface, and consequently improve the space time yield.

Reactor Wall and Catalyst Support: The materials applied for the reactor wall and/or catalytic support also have influence on the heat transfer property of the microreactors.

Common reactor wall materials are stainless steel (grade AISI/SAE 304 and AISI/SAE 316), alumina, silicon carbide (SiC), FeCr alloy, titanium, etc. Hosukoglu et al. modelled and simulated the thermal profiles of FT wax hydrocracking processes ($\Delta H_{STP} = -42$ [kJ·mol^{-1}]) using AISI/SAE steel (Thermal conductivity: 44.5 [W·m^{-1}·K^{-1}]), alumina (27 [W·m^{-1}·K^{-1}]) and SiC (87 [W·m^{-1}·K^{-1}]) as channel walls.[77] They found that the temperature rose versus the feeding temperature as 10, 3 and 0 [°C] for alumina, steel and SiC walls, respectively, along the 0.1 [m] microchannel under typical operation conditions, confirming that high thermal conductivity of the channel walls enables a high rate of heat removal from the reaction channel, thereby preventing steep temperature rises along the channel. Nevertheless, the choice of materials for better heat transfer is often a compromise among achieving high thermal conductivity, maintaining mechanical strength, robust inertness, pressure tolerance, corrosion resistance and minimizing capital cost, especially as the reactor scales up. Additionally, a wall thickness in the $3–4 \times 10^{-4}$ [m] range is recommended by several simulations on FT wax hydrocracking reaction,[77] coupled combustion/steam reforming[92] and FTS/cooling.[93] These indicate that thicker walls favor the heat flux in the flow direction of the solid wall and thus slow down the rate of temperature rise versus the feeding temperature along the channel. However, several experimental setups use thicker walls of $1–3 \times 10^{-3}$ [m][13,63,94] since from the practical operation point of view, the wall thickness of the reactor should also guarantee a safety threshold of high-pressure difference between reaction and cooling sides ΔP up to 30 [bar]). Thus, based on current experiences, a reactor wall with high thermal conductivity and thickness of 1×10^{-3} [m] is recommended to reduce the risk of hot spot formation along the microchannel/microtube.

Scaling Up: Sizing up and numbering up are the common strategies for scaling microchannel and microtube reactors.[29]

For sizing up, dimensionless groups such as *Nu* and *Re* numbers are usually considered as scaling criteria,[29] however, microreactor scaling up via cross-sectional sizing up is usually only limited within magnitude of 10^{-2}–10^{1} [mm]. This restraint is mainly to maintain the heat-transfer property of the microchannel and -tube. Analytic results from Kockmann et al.[95] and Chabot et al.[10] suggested that, for exothermic processes, there exists a critical hydraulic diameter of cylinder-shape reactors below which thermal runaway is avoided, and reactions with a characteristic reaction time below 1 [s], a diameter of 0.5–1.0 [mm] is favorable. Specially for FTS, a simulation work for the packed-bed microtubes (25%Co/0.1%Pt/Al_2O_3: 90 [μm]; space velocity: 20 [g_{syngas}·min^{-1}·$kg_{cat}$$^{-1}$]; cooling temperature: 493.15 [K]; molar ratio $H_2/CO = 2$; reaction rate ≈ 5 [s]) shows that a diameter < 3.12 [mm] is favorable. Besides, another experimental work suggests that the microchannels with a cross section of $d_h = 6.6$ [mm] for FTS process can sustain a cross-sectional temperature difference ≤ 3 [°C].[84] Thus, scaling-up of microreactors for sizes beyond these dimensions usually requires numbering-up, as discussed in the following.

During numbering up, heat removal can become crucial for exothermal reactions such as FTS process, since reaction heat from each microchannel or -tube may be accumulated and thus hot spot could be formed. Most of lab-scale single-channel set-ups seldomly apply active cooling strategies, expect a few studies,[13] owing to the fact that the heat release from restricted catalyst loading in one single channel or tube is limited. Generally, both the heat management of the numbering-up microchannels and the coolant channels for highly exothermic processes require optimal arrangement for an efficient FTS process. For this, three flow configurations, i.e., counter-current (flow directions of reactants and coolant are counter), co-current (flow directions of reactants and coolant are same) and cross-flow (flow directions of reactants and coolant are vertical), as illustrated in **Figure 7**, are summarized in one review elsewhere[27] and are reckoned as common strategies for effective heat exchange. Further experimental and simulation results reveal that the counter-current flow configuration has high heat exchange capacity and high temperature difference, while the co-current one has lower heat exchange capacity but more even temperature distribution.[27]

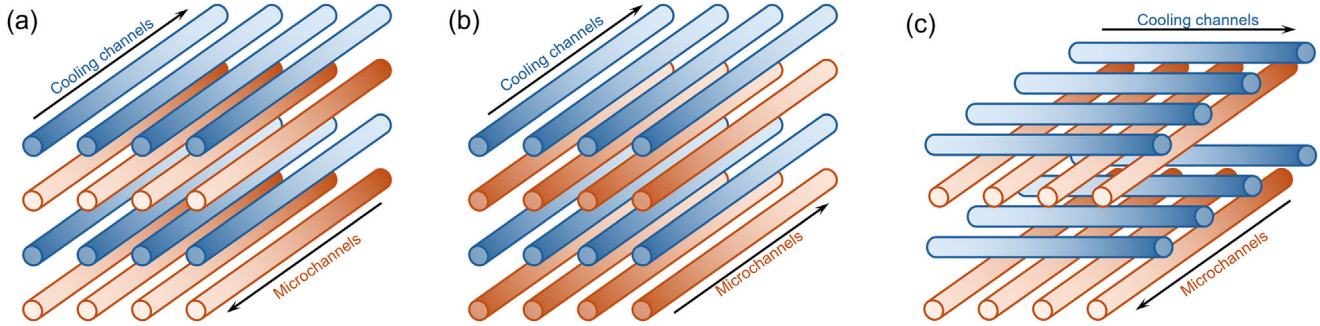

Figure 7. Three arrangements of microchannels and cooling channels: a) counter-current, b) co-current, and c) crossflow.

The performance of the crossflow lies between that of counter-current and co-current configurations. FTS pilot-scale or multi-channels often use the crossflow configuration (see Table 5), to achieve an acceptable trade-off between heat exchange capacity and temperature distribution. It should be noted that the pilot-scale FTS microchannel reactors from Karlsruhe Institute of Technology (KIT),[96] Velocys, Inc.,[13] Ajou University,[84] and Seoul National University[14,85] employed boiling water as a coolant, instead of hot oil which is used in the laboratory scale. One reason is that partial boiling conditions enable a large amount of heat removal through the water phase change without changing the coolant temperature too much, so that the reactor temperature also could remain relatively stable. However, the technical or mechanical challenges of applying partial boiling water as coolant are seldomly reported. Besides, uniform flow distribution (of both reactant and coolant) across numbering-up channels or tubes benefits the thermal performance and determines the efficiency of the heat removal/exchange. A summary of the design of flow distributors can be found in one review elsewhere.[29]

2.3.2. Mass Transfer

Mass transfer phenomena are complex in an FTS microreactor since the material, energy, and momentum balance for the gas, liquid, and solid phases as well as multi-phase mass transfer (e.g., gas–gas, gas–liquid, liquid–liquid, gas–solid, and liquid–solid) need to be considered simultaneously. A schematic for a reaction-diffusion-dispersion model of a simple heterogenous reaction process is given in **Figure 8**. From the macro-scale perspective, the reactants and products (gas and/or liquid) experience axial and lateral dispersion, while on a micro scale, the reactants undergo film diffusion – pore diffusion – absorption – chemical reaction – desorption – pore diffusion – film diffusion. Those processes could be even more complex in practice. As described before, the small dimensions of microreactors provide relatively short mass transfer lengths and thus excellent mass transfer characteristics. Besides, the flow pattern in microreactors is usually laminar, thus, "macro diffusion" or dispersion, which are more relevant for reactors of larger dimensions (e.g., SB, CFB),[97,98] play a minor role in microreactors.

For "micro diffusion", as seen in Figure 8, mass transfer of reactants to the catalyst surface microreactors can be distinguished between: i) internal mass transfer, representing transport of the reactant in the catalyst pores, and ii) external mass transfer, representing transport of the reactant (gaseous) through the phase (gaseous or liquid) films to the catalyst surface. In this review, gas–gas mass transfer is excluded since in such small dimensions of microreactors, the gaseous phase can be assumed as ideal gas (see Table 6), whereby further details are reported elsewhere,[99] however, the external mass transfer resistance due to the long-chain hydrocarbon, which is formed as liquid form, is not trivial, whereby more reports could be found for catalyst particles[100–102] while little information for wash-coated catalyst. Simulation considerations of mass transfer resistances in FTS microreactors are also not trivial (see Section 3.2), and indeed FTS product distribution and catalyst activity are strongly influenced by diffusion limitations,[39] especially after wax accumulation in catalyst pores.[100] However, most catalytic experiments

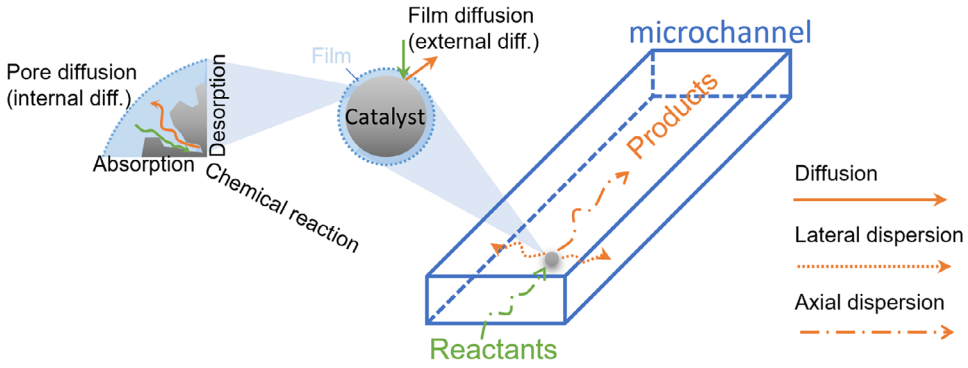

Figure 8. Schematic of mass transfer in a heterogeneous catalytic reaction process. "diff". is short for "diffusion".

are claimed and conducted in a regime of almost negligible mass and heat transfer limitation so as to determine the kinetic limitations and thus, offer limited information on the internal and external mass transfer.[61,63,103,104]

Due to the complexity of mass-transfer phenomena, experimental observations on CO conversion, methane and C_{5+} selectivity can be counterintuitive for FTS process. Typically, in conventional FB, the CO conversion decreases, and the methane selectivity increases with increasing catalyst particle size, however, this behavior can be changed and even have opposite effects due to the change of local H_2/CO ratio, liquid formation and drainage as well as hydrodynamic behavior.[61] Therefore, careful considerations of the mass transport within the catalyst, to estimate the appropriate reaction rate and product selectivity, are mandatory for development of simulation models that predict FTS reaction processes with acceptable accuracy. It should be noted that internal mass transfer depends more on catalyst design (e.g., material synthesis, etc., are excluded in this review) than on reactor design. Thus, the following sections introduce the design requirements of the catalyst dimension as well as microstructures in the reactor, channel wall surface and the catalyst support.

Catalyst Dimension: The "catalyst dimension", i.e., particle size (for packed-bed reactors), shape and catalyst thickness (for wash-coated ones), porosity, tortuosity, etc., can influence the pore diffusion, reactant adsorption, product desorption and active site exposure of the catalytic reaction. Inappropriate particle size can cause significant internal and external mass transfer limitations.

The particle size of the catalyst in the packed-bed microreactors ranges from 30 to 2 [mm].[4,10,13,14,64,65,96,103,105–107] Generally, smaller particle size brings less external and internal mass transfer limitations. For example, under typical FTS conditions, the corresponding Mears number for an Fe-based catalyst with a particle size 40 [μm] was found to be around 0.001,[103] which is smaller than 0.15, thus, indicating negligible external diffusional limitations. The calculated Thiele modulus under typical FTS condition of a powder catalyst with porosity 0.65, surface area 85 [$m^2 \cdot g^{-1}$] and tortuosity factor 2 was found 0.11, which is less than 1, thus, indicating elimination of negative internal diffusion resistance.[103] However, from a practical perspective, particle sizes of 80–100 [μm] seem optimal to minimize the mass transfer resistance in FTS without significant rise of capital cost and pressure drop and causing difficulty for liquid drainage (see Section 2.3.3). When larger particles are required to further minimize pressure drops, the catalyst pellets are coated with the active phase usually only as an eggshell layer of around 100 [μm] thick for effective catalyst usage.[106]

The thickness of the catalyst layer in wash-coated microreactors also has a significant influence on the mass and heat transfer and its values in literature range usually from 10 to 600 [μm],[51,53,54,61,63,73,76,107,108] and amongst many, a catalyst thickness ≤ 100 [μm] seems optimal for the catalyst effectiveness and heat removal in FT microreactors. Due to the compact catalyst loading and the small size of the catalyst in the wash-coated one the internal mass transfer limitation is more pronounced than its external mass transfer limitation.[107] Thus, the effects of microstructures upon the wash-coat surface on internal and external (i.e., when liquid is formed) mass transfer resistance are gaining increasing interest. Though a comprehensive and exact matching correlation for the description of these effects have not yet been developed, several researchers agree that fine pores (e.g., nanometer-sized) of the wash-coated catalysts additionally hinder diffusion in the liquid phase,[109–115] due to the increased external/internal mass transfer resistance and poor access of the reactants to the catalyst active sites in the pores. Considerably small microstructure (surface area: BET>10^3 [$m^2 \cdot g^{-1}$]) as catalytic support has been found to negatively affect catalyst activity.[116] Becker et al.[117] suggested that for catalyst layers with thickness 150–500 [μm], where mass transfer limitation is evident, transport pores with diameters of 1–2 [μm] in the layer are necessary to minimize the mass transfer resistances. Furthermore, for improvement of the diffusion inside the catalyst, a bimodal pore structure is proposed by Xu et al.,[109] through which larger pores can improve the accessibility of the catalyst for the reactants, and smaller pores provide high surface area and activity.

Nevertheless, it should be noted that catalyst pore size, porosity, tortuosity and surface area are more of catalyst design than of reactor design, though those parameters will to a certain extent affect the reactor design. In this regard, more in-depth investigations are still needed.

Reactor Dimension: As mentioned previously, the small dimensions of microreactors provide excellent mass transfer characteristics. It is an acceptable assumption when gas–gas reactions dominate, and catalyst activity is not infinitely fast.[60] For example, the diffusion rate of water, one of the slowest diffusing products, is found to be around 5 orders of magnitude higher than the observed reaction rate of CO/CO_2 hydrogenation at FT relevant conditions.[118] In this case, the second Damköhler number *Da* across a cross section with a dimension of 35 [μm] is of the order of 10^{-6}, indicating negligible gas–gas diffusion resistance. However, as the long-chain hydrocarbons, which are the main FTS liquid products, are formed, the difference on partial pressure, diffusivities and solubilities of reactants (i.e., CO and H_2) in the liquid can cause a change of local H_2/CO ratio, meaning accessibility of reactants to catalyst active sites is deviated from the reactor bulk region and thus a shift of products distribution as well as a change of heat release occur.

Generally, liquid drainage in wash-coated reactors is better than in packed-bed ones; moreover, increasing gas velocity would reduce the liquid film thickness. In one simulation work, the results indicate that the thickness of liquid film in a wash-coated FTS microchannel reactor with a reactor length > 1 [m] is predicted > 10 [μm].[73] Thus, to avoid liquid products forming slug flow regime, which blocks channel cross section and enhances pressure drop, the minimal cross-sectional dimension of FTS microreactors seems to be at least d_h > 50 [μm], or the height of the rectangular channel $H_{m.r.}$ > 50 [μm]. On the other hand, the liquid drainage in packed-bed reactors needs to be optimized by particle sizes as well as packing structures, which is further elaborated in the next section.

Microstructures: As mentioned above, "microstructures" of the reactor, opposed to the "microstructures" of the catalyst, refer to the packing structures in the micromonolith and microstructured reactors in Figure 2c,d. They provide potential for uniform temperature distribution as well as to decrease pressure drop (see

Section 2.3.3). A comprehensive comparison of the effect of different diffusion lengths on FTS in the conventional packed-bed reactor as well as packed-bed (various catalyst particle sizes) and wash-coated monoliths (various catalyst thicknesses) was experimentally carried out by Ibáñez et al.[61] They confirmed that an opposite behavior on CO conversion, methane, and C_{5+} selectivity as increasing catalyst particle size in monolithic packed-bed reactors compared to conventional packed-bed ones are observed. Besides, the packed-bed monoliths allowed a higher catalyst loading (0.82 [$g_{cat}\cdot m^{-3}$]) than wash coated monoliths (0.33 [$g_{cat}\cdot m^{-3}$]), yet, for the same monolith, the wash coated reactors despite their lower catalyst loading, achieved higher CO conversion and higher C_{5+} selectivity than the packed-bed variants. After eliminating significant difference on heat-transfer effects, they postulated that the reason for the marked difference in behavior of the conventional packed bed, packed-bed, and wash-coated monoliths is that the drainage of liquid improves from the first to the last, and waxy products are hindered more by the poorer gas–liquid contact with small catalyst particles (< 200 [µm] diameter) compared to wash-coated channels/monoliths, leading to much poorer radial transport/distribution of the reactants. However, further investigations on the effects of microstructure dimension and geometry on mass-transfer characteristics are missing. Therefore, the effect of varying reactor microstructures on the nature of mass and heat transfer is still unclear. This again suggests that the FTS process is sensitive toward the tuning of mass transfer and careful considerations in design are non-trivial.

2.3.3. Pressure Drop

The pressure in a microreactor affects the absorption process during chemical reactions whereby high pressure drops reduce the residence time and thus may cause the reaction rate and conversion rate to drop below optimal values. In terms of reactor design, one immediate consequence of a larger-than-desired pressure drop is that the active length of the reactor is shortened leading to low conversion rates and possible errors in scale up/down. Also, fluid dynamics have a significant impact on mass and heat transfer phenomena in microreactors, affecting the velocity profile (local observation) and the pressure drop (integral observation) through reactor design and operation conditions. Thus, practical realization of efficient reactors requires compromises: for example, packed bed catalysts with smaller catalyst particles tend to be more active than larger ones for FTS and allow higher loading, both of which would increase the space time yield/volumetric productivity of the reactor, however, the pressure drop may increase above acceptable levels. This is a particular problem when laboratory sized reactors with a comparatively smaller ratio of reactor to particle diameter are used to develop and to parameterize models for predicting the performance of industrial reactors. Moreover, in reactor design, a compromise must be made between achieving a low pressure drop (laminar flow) and a high heat transfer coefficient (turbulent flow). Therefore, pressure drop is of special interest for the scaling-up of reactors.[29,95] Additionally, knowledge of the pressure drop is needed to economically size the auxiliary equipment such as pumps, recyclers, and compressors for industrial reactors, to maximize utilization of the syngas feed.[119]

The pressure drop in packed-bed and wash-coated reactor can be described by Ergun equation and Bernoulli equation, as given in Equations (14) and (15). It should be noted that the friction factor C'/Re^n can also describe the overall pressure loss for both Equations (14) and (15), and the values of this term for packed-bed and wash-coated microreactors might be quite different, however, limited attention is paid to this difference for reactor design in the literature. According to Equations (14) and (15), those parameters, i.e., bulk porosity (catalyst loaded as packed bed), catalyst holdup, particle size and shape, channel geometry, surface roughness and microstructure in the reactor, liquid holdup, space velocity and flow distribution, affect the flow profiles and the pressure drop in microreactors, and the following sections will elaborate their design parameters and the role in the design of FTS microreactors.

Catalyst Loading: Different catalyst loading methods (see Figure 4) change the permeability and porosity of the reactor, determining the structure of the reactor channels. It is widely accepted that to maintain effective heat removal in a laboratory-scale packed-bed microreactor the pressure drop under typical FTS conditions should not exceed 1.5 [$bar\cdot m^{-1}$].[72] Exemplarily, the pressure drop in one FTS microchannel (depth × width × length: 1 × 1 × 40, [mm]) with packed particle size 40 [µm] at space velocity 5–8 [$L\cdot g_{cat}^{-1}\cdot h^{-1}$] ranges from 0.2 to 1.2 [$bar\cdot m^{-1}$];[103] the pressure drop of a packed-bed microtube (i.d. × length: 1.753 × 1000, [mm]) with packed particle size 140–200 [µm] at space velocity 0.012–0.053 [$m\cdot s^{-1}$] ranges from 1.22 to 1.37 [$bar\cdot m^{-1}$]

In general, the pressure drop for wash-coated microreactors is one to three orders of magnitude lower than packed-bed ones, i.e., 10^{-3} [$bar\cdot m^{-1}$],[61] and thus, only a minor issue in terms of design. For example, the pressure drop of a pilot-scale plant for hydrogen production from steam reforming of methane at 5 [$Nm^3\cdot h^{-1}$] in a microchannel system using wash-coated monolith was reported around 0.7 [bar].[120] However, due to such low pressure drop in the wash-coated microchannels or -tubes, poor uniformity of gas distribution during channel or tube numbering up might arise, whereby the gas flows tend to bypass the channels or tubes where a slight increase of pressure drop from mainly manufactory errors exists. It is rarely discussed in the literature, rather, a variety of investigations on flow uniformity among liquid-based channels are reported.[29] Due to its relatively higher Schmidt number *Sc* (see Equation (9)) of liquid compared to gas, the results of flow uniformity of room-temperature channels with liquid as media make it difficult to interpret the behavior of gas flow uniformity, and thus, more studies are still needed.

Channel Geometry: For a packed bed, given constant reactor length, particle size, bed density and flow rate, the pressure drop is independent on the diameter of the reactor, while for a wash-coated one, the smaller the channel dimension is, the greater the pressure drop will be, as seen in Equations (14) and (15). Thus, channel geometry is more a factor for pressure drop in wash-coated microreactor than in packed-bed ones. As shown in Equation (15), the friction factor C'/Re^n is dependent on flow conditions and channel geometry. For laminar flow in a straight empty channel, $n = 1$; for fully turbulent flow (i.e., $Re > 10^4$), $n = 0$;[121] however, Dong et al.[29] suggested that $n = 0.25$ should be used in microreactors in the *Re* range between 100 and 4000. On the other hand, the effects of channel geometry on the viscous and

kinetic constants (i.e., E_1 and E_2 in Equation (14)) are seldomly reported in literature.

Surface Roughness and Microstructures: The effects of channel surface roughness and microstructures on the flow fields and pressure drop of a reactor vary according to the catalyst loading method used.

In packed-bed reactors, apart from random packing of the catalyst, microstructures in the reactor volume, such as CCFS structures (see Figure 3h), can offer good catalyst holdup, which changes the particle loading pattern as well as flow pattern. Experimental and simulation results showed that such structured packing can reduce pressure drop losses compared to conventional randomly packed reactors.[64,65] It is because the microstructures rearrange the packing pattern, decreasing the total loading mass of the catalyst and consequently increasing the overall porosity as well as lowering the flow friction, thus, decreasing the pressure drop, as described in Equation (14). Moreover, experimental results show that the gas velocity in a packed CCFS microreactor can be around 30% higher than that in random packed-bed ones in the same pressure drop range 0.05–0.15 [bar·m^{-1}], i.e., a lower pressure drop at the same gas velocity.[64] Though the total catalyst loading decreases, results also showed that FTS productivity can be increased. Besides, the pressure drops of reactors can also be reduced by using regular shaped catalyst forms.[122] In contrast, surface roughness has a negligible effect on pressure drop in packed-bed microreactors for gaseous reactants.[91]

However, the wall roughness ($H_{m.st.}/H_{m.r.} < 10^{-3}$), confinement and wettability play an important role for the fluid dynamics in wash-coated microreactors.[31] A surface roughness of 10^1–10^2 [µm] was found to enhance formation of secondary flows and eddies in contrast to smooth surfaces (see Section 2.3.1), nevertheless, the effect on the pressure drop in wash-coated microreactors is negligible.

As mentioned above, packed-bed reactors enable more catalyst inventory compared to wash-coated ones. Thus, to increase catalyst loading in wash-coated microreactors to enhance catalytic performance and to make good use of the free-flowing volume, a microstructure is recommended, which usually has higher porosity than random particle packed-bed system. Then, the catalyst is coated on the surface of these microstructures (see Figure 2c,d). In this case, the pressure drop will increase due to the microstructures (i.e., the increase of pack porosity ϵ compared to free-flowing empty channel) but is still much lower than packed-bed catalyst loading. The change of bulk porosity ϵ via introducing microstructures in the wash-coated microreactors might lead to a shift in applying Equation (15) to (14), however, it is yet to be in-depth discussed in the literature.

Fluid Density and Distribution: Generally, fluids in packed-bed reactors and microstructured reactors approximately follow Darcy's law, which describes the flow of a fluid through a porous medium.[10] Specifically, flows for FTS reactors with liquid products operate in the trickle-flow regime.[107] Liquid holdup can increase pressure drop along the reactor length by contributing to ρ_f in Equations (14) and (15). In the worst case, blocking of cavities in the microstructures and catalyst bed may occur, increasing the risk of thermal runaway. However, related information is seldomly reported in literature. Nevertheless, for microreactor designs good liquid drainage is important for safe operation. Besides, as would be expected in a multi-channel reactor, the pressure drop of each channel determines the flow uniformity of the whole unit. Thus, non-uniformity related to liquid formation should be also taken into consideration.

2.3.4. Residence Time Distribution

Residence time distribution (RTD) describes essentially a fluid element spending a certain amount of time inside the reactor system before exiting. It is an important concept used in reactor design to ensure not only sufficient residence time of the reactant molecules/atoms but also the selectivity of the products. For the overall reactor dimension the lengthwise $Da \geq 10^0$–10^1 should be targeted for sufficient conversion (see Section 2.1). However, not all the reactant molecules/atoms travel through the reactor identically, i.e., some are faster, and others are slower. As such, transport difference of each fluid component will lead to local variance on the absorption and desorption of reactants and products during the catalytic processes. Subsequently, a change in product selectivity could occur. Therefore, proper reactors should maximize the contact between reactants and active sites as well as ensure an efficient removal of the products, for the catalyst to perform with almost intrinsic kinetics.

The residence time and RTD are usually measured via tracer methods.[40] Exemplarily, Boskovic and Loebbecke[123] developed a technique for the measurement of the RTD in the microfluidic devices by using a spectroscopic method to monitor an input–response signal, where the deviations caused by the connected capillaries and their contribution to the overall RTD were considered based on modelling analysis. In another method, the difference between "residence time" and "contact time" in a packed-bed reactor was distinguished by Orth and Schügerl[124] after considering ethene-hydrogen reaction on a palladium catalyst.

However, it should be noted that "residence time" and "contact time" in microreactors are often treated as equal in the literature, though they are termed differently.[13,125] For example, Tonkovich et al.[33] defined contact time as being equal to (open channel volume)/(flow rate at standard temperature and pressure) for a wash-coated microstructured reactor, i.e., the reactant flows *by* not *through* the catalyst and the foam region with catalyst was neglected – causing a difference on V in Equation (16). And in most of the FT experimental works, contact time is usually a normalization of the feed rate to a catalyst property, e.g., gas hourly space velocity (GHSV, [$m_{reactant}{}^3 \cdot m_{cat}{}^{-3} \cdot h^{-1}$] or often also [$ml_{fluid} \cdot g_{cat}{}^{-1} \cdot h^{-1}$]) and gas weight hourly space velocity (WHSV, [$g_{reactant} \cdot g_{cat}{}^{-1} \cdot h^{-1}$]). It should be also noted that these contact times are often given under 0 [°C] and 1 [bar] (International Union of Pure and Applied Chemistry (IUPAC), and may vary if other standards are applied, e.g., National Institute of Standards and Technology (NIST)), instead of operating conditions – causing a difference on ν in Equation (16). Thus, it is often difficult to compare residence times or contact times for different experiments reported in the literature. However, due to the small channel dimensions, microreactors usually exhibit a narrow RTD, i.e., $Bo \geq 10^2$ (see Section 2.1), which is desirable to ensure that the reactants have very similar residence/contact time, to prevent subsequent reactions toward undesired by-products. Thus, in the current review, the two extreme cases, i.e., narrow and maximal broad RTDs by an ideal plug flow reactor (PFR)

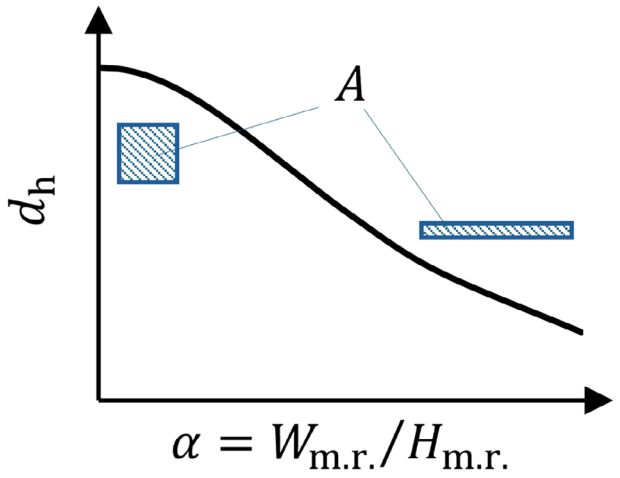

Figure 9. Change of hydraulic diameter d_h with increasing aspect ratio α at fixed cross-sectional area A.

and an ideal continuously stirred tank reactor (CSTR),[40] are discussed. For catalytic kinetics study, usually either PFR or CSTR reactors are employed, whereas applied reactors usually lie somewhere in between.

PFR: The PFR model assumes that the reactants are ideally repressed along the reaction axis, resulting in an infinitely narrow RTD and high space-time yield. Microreactors in simulation are usually treated as ideal plug flow reactors,[10,62,63,106,107,126] and most of them are usually packed-bed reactors. Despite most likely having a laminar flow profile, it is a reasonable assumption since due to their small dimensions and finite reaction rate the concentration gradients across the cross section in the microreactor channels are very small and often negligible. However, several simulation works show that microchannels with infinitely fast wall reactions (e.g., by wash-coated catalysts) cannot be treated as 1D PFR model,[58–60] rather, cross-sectional mass transfer should also be considered. When the corner effects start to play a prominent role, 3D model might also be demanded. Moreover, their results also indicate that the velocity profile of the inlet (i.e., laminar or plug-flow pattern) can also affect the reaction conversion at the exit, which is often neglected in PFR assumption. Nevertheless, the extent of the error caused by this approximation for specific applications in microreactors is, however, case dependent and needs to be investigated individually.

Combination of PFR and CSTR: For perfect back mixing of reactants, CSTR behavior is desirable, to e.g. avoid side reactions occurring at high initial reactant concentrations or managing the heat of highly exothermic reactions at the reactor inlet. However, it is hard to achieve either of the two extreme cases in practice, therefore, the actual RTD in real reactors can be assumed as a combination of PFR and CSTR. Aubin et al.[125] through simulation investigations using non-Newtonian and Newtonian fluids suggested that, to obtain a narrow RTD and reduced axial dispersion, the microchannels should be designed with large aspect ratio $\alpha \geq 3$ for a fixed cross-sectional area. In their simulation, reactions are excluded. However, as presented in **Figure 9**, increasing of aspect ratio α leads to a decrease of hydraulic diameter d_h as well as increase of flow velocity (i.e., flow rate is fixed), thus subsequently, an increase of pressure drop (see Equation (15)). Besides, very large α (i.e., very small $H_{m.r.}$) can largely increase the risk of channel blockage, especially for FTS process, as discussed in Section 2.3.2. Since the temperature uniformity of a rectangular geometry with $\alpha = 0.5–3$ is satisfactory (see Section 2.3.1) and the pressure drop should be controlled within a reasonable range, $\alpha = 0.5–3$ is more appropriate for FTS process which targets especially for long-chain hydrocarbons, while $\alpha > 3$ or $\alpha < 0.5$ is more suitable for gas-phase processes.

Combining both CSTR and PFR can be beneficial for process optimization. Based on simulations, Rafiee and Hillestad[126] proposed a two-staged design of an FTS reactor using a CSTR reactor in the first stage and a PFR in the second stage. The CSTR stage serves to level out the temperature peak due to the initial high reaction rate and larger reaction enthalpy of the FTS while the PFR stage, being more efficient in terms of space-time yield, increases the productivity of the proposed process. Simulations revealed that by proper combination of both, the wax production could be increased by 2% and the CO conversion by 2% while keeping the peak temperature rise in check. However, whether such a concept can be practically transferred to microreactors is questionable, as significant back-mixing in microstructures is nearly impossible.

2.4. Summary and Discussion

To achieve a high C_{5+} selectivity and CO conversion rate for FTS, design strategies should reconcile the conflicting requirements for high heat and mass transfer rate, low pressure drop, and appropriate residence time. In this section, the core relationship between design parameters and the dimensionless numbers is summarized in Table 2, and based on the findings above, the design boundaries for FTS microreactors are discussed, as well as the preliminary comparison of design parameters (i.e., hydraulic diameter and length) from engineering perspective between FTS and other syngas-related processes. Finally, the design and operational parameters of existing pilot-plant microchannel reactors for FTS are also summarized.

First, the hydraulic diameter d_h is an important design parameter for heat transfer (described by Nusselt number, see Equation (6)) and mass transfer (described by Sherwood number, see Equation (8)), as summarized from the literature in the sections above, since it determines Reynolds number direct-proportionally (see Equation (5)) – indicating flow hydrodynamics in the reactor – at given operational conditions. It is because flow hydrodynamics forms the basis for heat and mass transfer in one reactor, thus, both Nusselt number and Sherwood number have strong correlations to Reynolds number. As seen in Table 2, due to the cross section of 10^{-2}–10^{1} [mm] for microreactors, *Re* is in a range of 10^{0}–10^{2}, and subsequently, most of the dimensionless numbers are limited to a certain range of values. However, due to the inherent difference in flow hydrodynamics for different catalyst loading methods, heat and mass transfer phenomena in the packed-bed and wash-coated reactors are also quite distinct and the challenges to overcome are also different. Specifically, for exothermal reactions in the packed-bed one, to avoid hot spot or thermal runaway (i.e., for heat transfer) is extensively focused. For this, a critical hydraulic diameter (i.e., upper limit) should be underlined. It can be roughly estimated by reaction rate, reaction enthalpy and cooling strategy. Exemplarily, under

Table 3. Cross-sectional dimension of packed-bed microchannel reactors for five exothermic processes.

Process[a)]	Enthalpy [kJ·mol^{-1}][b)]	Reaction rate [mol·m^{-3}·s^{-1}][c)]	Temperature rise [°C·mm^{-2}]	Critical hydraulic diameter [mm][d)]
FTS[79,131]	170.9	8.0	0.14	6.8
CO_2-to-methanol[132,133]	55.9	7.5	0.04	12.4
CO-to-methane[134,135]	225.1	6.1	0.16	9.9
CO_2-to-methane[134,136]	176.3	7.7	0.14	7.0
CMC of methane[137,138]	813.3	12.7	1.03	2.5

[a)] Bed thermal conductivity is assumed 10 [W·m^{-1}·°C^{-1}], bed porosity is 0.4, catalyst dilution with inert is ≈50 wt%, catalyst true density is 1000–1700 [kg·m^{-3}]. [b)] Enthalpy under typical operation conditions of a given reaction. [c)] Initial reaction rate or reaction rate under high activity region. [d)] Threshold cross-sectional dimension evaluated under high catalyst activity; definition as given in Equation (4).

typical FTS condition, to avoid thermal runaway, a hydraulic diameter for one microchannel or -tube approximates ca. 6.8 [mm] (see **Table 3**) according to our calculation, which is also consistent with 2D mathematical FTS calculation done by Chabot et al.[10] Furthermore, in their study, another example applied with cooling strategy indicated that a hydraulic diameter < 3.12 [mm] is favorable.[10] On the other hand, the hydraulic diameter of wash-coated microreactors can be comparably smaller than packed-bed ones due to two main reasons, i.e., wash-coated ones load less catalyst than packed-bed ones and thus generate less reaction heat; free-flowing volume should be better used by decreasing the overall size of the reactor system. However, a lower limit exists when liquid drainage (i.e., mass transfer) and pressure drop are considered. As mentioned above, to avoid liquid products forming slug flow regime and subsequently blocking channel cross section, d_h > 50 [µm] or $H_{m.r.}$ > 50 [µm] for FTS process seems applicable. Nevertheless, the lower limit depends on catalyst activity, wash-coated thickness and operation conditions, i.e., how much liquid is formed. Thus, based on findings above, we suggest that a ratio of wash-coated catalyst thickness and hydraulic diameter lies in a range of 0.15–0.2 [mm·mm^{-1}][61,73,107] with consideration of catalyst thicknesses ≤ 100 [µm] to minimize mass transfer limitation in catalyst layers. A ratio > 0.4 [mm·mm^{-1}] could lead to diffusion limitation and waste of catalyst.[63] Apart from hydraulic diameter as dimensional design, the design of cross-sectional geometry can also contribute to temperature uniformity. Though a rectangular geometry of $\alpha \geq 3$ is recommended for higher *Bo* (i.e., less axial back-mixing), in view of liquid formation during FTS process and to reduce the risk of channel blockage, an aspect ratio α between 0.5 and 3[13,14,51,55,75–78] is sufficient for reasonably narrow RTD profile as well as heat exchange, as seen in Table 2.

Second, the length of the microreactors can be estimated via Damköhler number (more specifically, the first Damköhler number Da_I), as discussed in Section 2.1. According to our calculation, for a packed-bed FTS reactor, CO conversion ≈70% usually requests a Damköhler number of ≈0.68 (see **Table 4**). Due to equilibrium effects, Damköhler number >> 1 will not further guarantee complete CO conversion, and thus, longer length is not necessary. Regarding channel geometry, the zigzag,[53] sinusoidal[55,56] and complex[57] shapes can enhance heat and mass transfer through creating turbulence and secondary flows, which seems favorable to many gas–solid catalytic processes. However, such effects on Nusselt number are limited.[55] Moreover, for effective liquid drainage (especially FTS process), the straight geometry for the microchannel/microtube is most favorable.

Additionally, design transfer from FTS to other syngas-related processes from engineering perspective, taking hydraulic diameter and length as example, is also conducted here. According to our calculation, as shown in Table 3, the critical hydraulic diameter for CO_2-to-methanol process is around 12.4 [mm], the CO-to-methanol process = 9.9 [mm], CO_2-to-methane process = 7.0 [mm] and catalytic methane combustion (CMC of methane) = 2.5 [mm]. Thus, in terms of heat removal capabilities, microreactors for FTS (d_h ≈ 6.8 [mm]) could be applicable as well for CO_2-to-methanol, CO-to-methane and CO_2-to-methane reactions but not for catalytic methane combustion. It is because the reaction enthalpy and the rate of the latter are much higher than FTS process. Therefore, the hydraulic diameter

Table 4. Damköhler numbers and reactor performance relevant to different gas-to-X reactions.

Process	Catalyst/loading [a)]	Temperature [°C]	Pressure [bar]	Reactant [mol·m^{-3}]	Contact time [b)]	*Da* [c)]	Conversion [%]
FTS[13,139]	Co/PB	210	24	CO: 124.7	4.2 [s]	≈0.68	≈70
CO_2-to-methanol[132,133,140]	Cu/PB	240	80	CO_2: 450.0	16.4 [s]	≈0.27	n.a.
CO_2-to-methane[86,134,136]	Ni/PB	400	9	CO_2: 26.8	110.8 [s]	20–30	≈90
SR of methane[33,141]	Rh/WCM	835	13	CH_4: 27.4	13.3 [ms]	≈12.7 [d)]	≈70
CMC of methane[138,142]	Pd/WC	450	1	CH_4: 0.2	0.2 [s]	≈3.85	>80
CMC of methane[137,143]	Pd/PB	300	1	CH_4: 0.2	37 [ms]	≈2.23	>90

[a)] Catalyst loading methods: PB-packed-bed; WC-wash-coated; WCM-wash-coated microstructure reactor. [b)] Recalculated based on reactor volume and operation conditions in literature. [c)] First Damköhler number, definition as given in Equation (13); reaction times based on reaction rate can be referred to Table 3. [d)] Highly active catalyst[141] was coated on foam in the reactor.

Table 5. Comparison of performance of pilot plant microchannel reactors for FTS.

Refs.	Velocys[13]	KOGAS[14]	Ajou University[15]	INERATEC[16]
Capacity	1.5 BPD	0.5 BPD	0.2 BPD	2 BPD
Catalyst	Commercial not disclosed	12 wt% Co/γ-Al_2O_3	Pt-Co/Si-Al_2O_3 catalyst	Commercial not disclosed
Catalyst form	Packed bed using 275–300 [µm] diameter particles	Packed bed using ca. 1 [mm] diameter particles	Packed bed, particle size not disclosed	Packed bed using 50–200 [µm] diameter particles
Scaling	276 channels @ •3.0 [mm] wide •171 [mm] catalyst bed length •1.0 [mm] gap as height	528 channels @ •10 [mm] wide •5.0 [mm] height •460/400 [mm] reactor/catalyst bed length	135 channels @ •Width and height of channels undisclosed •362 [mm] reactor length	Not disclosed
Coolant	Boiling water	Oil	Water	Water
H_2:CO	2.0	2.08	2.0	2.1–2.5
GHSV	12 400 [h^{-1}] (150 g_{cat})	2500 [$ml \cdot g_{cat}^{-1} \cdot h^{-1}$]	6600 [$ml \cdot g_{cat}^{-1} \cdot h^{-1}$]	100–125.4 [slm [b)]]
Pressure	24.13 [bar]	20 [bar]	20 [bar]	20 [bar]
Temperature	210 [°C]	220 [°C]	225 [°C]	202–216 [°C]
Lengthwise ΔT	±2 [°C]/300 [mm]	ca. 12 [°C]/460 [mm]	Not disclosed	Not disclosed
Average pressure drop	Not disclosed	2 [bar]/400 [mm]	Not disclosed	Not disclosed
Contact time	290 [ms]	Not disclosed	Not disclosed	Not disclosed
CO conversion	71.8%	83%	74%	50–60%
CH_4 selectivity	8.9%	50.13% [a)]	10%	5–30%
C_{5+} selectivity	85.2%	Not disclosed	81.3%	Not disclosed

[a)] Attributed to a low contact time of the reactants. [b)] Standard liters per minute.

should be around three times smaller than FTS microreactor to avoid hot spot formation or thermal runaway, or active cooling strategies should be applied. On the other hand, rough ranges of Damköhler number are also estimated for comparison, as given in Table 4. This can help to evaluate the adaptability of a reactor for one specific catalytic reaction as well as to estimate the suitable operation conditions (e.g., space velocity). Typically, in the packed-bed reactor for CMC of methane, a Damköhler number ≈2.23 results in CH_4 conversion > 90%. In contrast, a Damköhler number of 20–30 for a packed-bed reactor under CO_2-to-methane condition is unnecessary, where reaction might not occur at the channel downstream because the equilibrium CO_2 conversion is around 20–30%, and thus, larger residence time or longer channel length will not enhance conversion.

Interest has been shown on microstructures in the microreactor, which in this review indicates 3D volumetric microstructures in the reactor (see Figure 3c,d,h,i) and the microstructures on the reactor surface where catalyst is wash-coated (see Figure 3e–g). For packed bed, 3D microstructures alleviate the conflict between large catalyst loading for high space time yield and consequent high pressure drop.[64,65,127,128] As packing structure as well as heat transfer media, volumetric microstructures reconstruct catalyst packing pattern, flow profiles and temperature distribution, which results in higher catalyst usage and improved FTS-product selectivity.[64] For this, we summarize that a microstructure porosity around 0.85–0.95 with dimension of 50–1000 [µm][63,64] are sufficient. Besides, the impacts of microstructures on FTS liquid product formation have gained increasing interest yet further investigations should be expected. On the other hand, for wash-coated microreactors, catalyst has higher catalyst utilization than random packed beds[61] due to efficient heat removal, low pressure drop and better drainage of liquid and waxy products, though the total catalyst loading is lower. Thus, it is worth paying attention to surface- and volume-wise 3D microstructures (see Figure 3) for wash-coated microreactors, which can increase total catalyst surface area and catalyst loading, create flow turbulences and intensify heat transfer, compared to a plain wash-coated microchannel/microtube. As presented in Table 2, adding microstructures can change heat transfer (*Nu* number), mass transfer (*Sh* number), and flow hydrodynamics (*Bo* number). However, the mechanism is seldom discussed in literature. In this regard more investigations are still needed.

Nevertheless, temperature difference (cross-section-wise or length-wise) of $\Delta T \leq 3$ [°C] should keep in check for FTS microreactors.[61,84] Specifically, the lengthwise temperature difference of 0.002 [$°C \cdot mm^{-1}$] should also be constrained.[61,84] It is usually easy to achieve in lab-scale (either packed-bed or wash-coated) microchannel or -tube reactors, since the total catalyst inventory is small. But it can be an important overall criterion for sized-up or numbered-up microreactor set-ups. Regarding reactor material for better heat transfer, stainless steel is the most common reactor material, and other candidates are alumina, silicon carbide, FeCrAlloy, titanium, etc. Though high thermal conductivity of the materials is a key parameter mainly for higher heat transfer efficiency, mechanical strength, inertness, pressure tolerance, corrosion resistance and capital cost should also be borne in mind.

Finally, examples of pilot-scale microreactors for FTS process are shown in **Table 5**. Indeed, scaling up microreactors is usually realized by numbering up channel or tube units. The dimensions of microreactors vary within a limited range in order to maintain mass or heat transfer properties and results

from experiments and simulation indicate that within these dimensions the effects of geometry on the CO conversion are negligible,[13,19,75,116,129] while the effects on the product selectivity can be significant and even may be magnified during numbering up. As also seen in Table 5, a special attention is paid on heat management, i.e., crossflow cooling configuration is applied. However, the technical or mechanical challenges to applied partial boiling water as coolant is seldomly reported. Neither is the experimental details on gas uniformity among all units often reported, where the gas flows tend to bypass the channels or tubes where a slight increase of pressure drop from manufactory errors or catalyst loading difference exists, however, the results of flow uniformity of room-temperature channels with liquid as media fall short to interpret the behavior of gas flow among channel units under relevant reaction conditions. These impacts may in turn alter the reactant distribution, heat evolution, products selectivity and overall reaction rate. Besides, during FTS process, blocking of cavities in the microstructures and catalyst bed may occur, increasing the risk of thermal runaway, yet related information and their challenges are seldomly reported in the literature.

3. Challenges and Outlook

Though a substantial amount of work has already been published on microreactors for FTS and other applications, as discussed in the previous sections, there are still a few open questions and challenges to be overcome. In the following section limitations of existing experimental and simulation work are discussed, and opportunities for future research are outlined.

3.1. Experimental Limitations

In microreactors, the effects of heat transfer, mass transfer, flow field and pressure drop, residence time and distribution are usually interrelated, and experiments are not able to easily disentangle their effects. Quite often, only the temperatures at specific locations such as the inlet, middle of the reactor and the outlet are measured, which may not sufficiently capture the evolution of the heat distribution and transfer phenomena during reacting operation, especially for numbered-up microreactors. Also, for microreactors, concentration profiles in the axial and especially lateral directions are largely unavailable experimentally. A lack of accurate concentration profiles limits the understanding of the effects of reactor design, operation conditions, catalyst, etc. on performance and scale-up. Therefore, for selectivity-sensitive catalytic reactions, e.g., FTS, *operando* measurements that spatially resolve concentration and temperature gradients at such small scales, are imperative. For resolving temperature gradients in microchannels, thermographic imaging might be possible in certain cases,[144] but high-resolution measurements of flow and concentration profiles are complex on such small scales. While flow profiles, especially in liquid phase reactors, at room temperature can be easily captured using microscopic particle image velocimetry (micro-PIV),[37,57] they are yet measurable neither for gas-phase reactions nor in *operando*. It could be problematic if the intrinsic kinetic data of the catalyst should be extracted, but the flow pattern is far away from an ideal flow pattern, i.e., PFR or CSTR. Additionally, experimental measurements of the residence time distribution in microreactors are also seldom reported.

Though mass transfer limitations have been observed in experiments, as seen in Section 2.3.2, the measurement data of the internal and external mass transfer in reactors are seldom reported. Instead, the concentrations of reactants and products are measured, and a theoretical analysis (e.g., Mears criterion and Thiele modulus) is applied to determine the transfer resistance.

For microreactors, precise quantification of products of GtL processes can be challenging, and often mass balance is difficult to achieve for small-dimensioned setups. This can cause in deviations when intrinsic kinetic model parameters should be extracted from experiments or when a simulation model may need to be validated.

Lastly, even for accessible experimental reactor data that is published, experimental conditions (e.g., liquid formation and channel blockage, gas flow non-uniformity in the multichannel) are not fully disclosed. This lack of information provides serious implications for the reactor design. Additionally, reliability as well as measurement accuracy makes both the calibration and validation of the simulation models, with high accuracy and predictive power, difficult.

3.2. Simulation

Numerical modelling is used to overcome the limitations in experimental tests and to improve the understanding of the phenomena of heat and mass transfer and flow hydrodynamics. It is also a mandatory tool for scaling up reactors. The quality of reactor simulation models strongly depends on the measurements from experiments in two ways: i) reaction kinetics and ii) model validation. However, because of the inaccessibility of experimental data, the expense and complexity of the necessary experiments to collect calibration data for models, among others, many assumptions are used for microreactor simulations. **Table 6** summarizes common assumptions for simulations and their implications for the accuracy and predictive power of the associated models. Deviations that arise from these common assumptions are seldom discussed in literature.

To disclose phenomena of heat and mass transfer via simulation, kinetic and selectivity models as well as mass transport models are very important. A summary of FTS kinetic and selectivity models applied in the literature is presented in **Table 7**. Most of the kinetic models are empirical and semi-empirical. Though empirical models can capture and describe the main features of experiments, their validity is limited to specific operation conditions. Thus, such models can result in low accuracy in predicting performance and fall short to scale up other types of reactors. On the other hand, semi-empirical models mostly refer to the kinetic mechanism based on Langmuir–Hinshelwood (L–H) or Langmuir–Hinshelwood–Hougen–Watson (LHHW) approaches. Corresponding experiments are carried out within a certain operating range, and kinetic parameters are obtained by fitting experimental data with L–H or LHHW model. When applying semi-empirical ones, it is important to check the conditions for which the

Table 6. Commonly used assumptions and their implications for microreactor simulation models.

Aspects	Assumption	Implications
Gas phase behavior	-Gas behavior obeys the ideal gas law and Henry's law.	-This assumption is valid at relatively low pressures (< 1 [bar]) and high temperature (>500 [°C]). -Deviations could arise under the operation conditions for a given catalytic reaction or liquid products are formed, and corresponding considerations should be made.
Operating conditions	-Steady state	-Catalyst undergoes deactivation in practical application. When deactivation is fast, this assumption could bring deviations.
Catalyst conditions	-No addition or removal of catalyst. -Catalyst does not degrade.	-Catalyst may experience deactivation via sintering, carbon deposit, build-up of waxes (for FTS), etc. -Concentration/temperature profiles change due to the addition/removal of the catalyst.
Temperature /concentration gradient	-Radial/cross-sectional temperature and concentrations gradients are neglected for 1D and pseudo-2D simulations.	-Laminar flow patterns in reactors indicate that heat conduction is dominant. -Cross-sectional temperature/concentration gradient indicates serious implications on the design of reactors for selectivity sensitive processes such as FTS, especially when catalyst reaction rate is quite fast.
Constant parameterization	-Constant physical properties of some reactants/products -For FTS, one single *n*-paraffin as C_{5+}	-Low predictive accuracy as dynamic phenomena, which vary with the operating parameters as well as with time and space, are not well described.

kinetic experiments are valid for reactor design and analysis. The current state-of-the-art simulation models can solve several independent and coupled processes simultaneously, but for that, more mechanistic-based reaction kinetics are necessary to develop a comprehensive model. Obtaining such models, however, requires extensive experimental work over a broad parameter range, coupled with *operando* spectroscopic methods. Besides, due to complexity of gas–liquid–solid reaction environment, long-chain product selectivity, simultaneous investigations on heat and mass transfer, hydrodynamics, and reaction performance are seldom conducted in the literature.

On the other hand, mass transport and diffusion of the reactants to catalyst active sites are modelled by mass transfer models. In the current literature, models for both internal and external mass transfer resistances during FTS process are developed. For internal mass transfer, wash-coated micro- and monolith-catalysts are assumed to be flat geometry, while for slurry bed columns and packed bed the catalysts are assumed be spherically shaped. Amongst many, pore diffusion model is often applied, where effective diffusion coefficient depends on tortuosity $\tau_{cat} = 3$ and catalyst porosity ϵ_{cat} and reaction rate is the driven force.[39,64,73,107,117,145] Quite informative results of H_2/CO ratio, reaction rate, and product distribution along the catalyst radius of one particle can be obtained, whereas temperature is assumed to be uniform and catalyst is fully saturated with a liquid medium. On the other hand, for external mass transfer resistance, empirical gas–liquid[65,146–149] and liquid–solid[39,65,150] Sherwood correlations as well as overall correlations based on direct numerical simulations (DNS) results[45,108] are reported in the literature. Quite often, these models coupled with reaction/kinetic models as well as other modeling phenomena, make the reactor simulation very computationally heavy, and the simulation fails to reach convergence. There are still many investigations needed to achieve the compelling goal of a "virtual replica" of the reactor through CFD modelling.

3.3. Future Investigations and Outlook

3.3.1. Controllable Micro-Structuring

Increasing interest in microstructures has been shown in the current literature, since it has been found that microstructuring can enhance heat and mass transfer, adjust flow profiles, decrease pressure drop and increase catalyst inventory, as mentioned above. Though a few works showed that microstructures have impacts on CO conversion, methane and C_{5+} selectivity for FTS process,[61] further investigations on the mechanisms of microstructure dimension and geometry impacting heat- and mass-transfer characteristics are still missing. Technically, the catalytic pellets, coated with highly porous catalyst powders and packed randomly in the reactor, which is often applied to reduce pressure drop of the packed bed, could also provide a "microstructure" in the reactor, i.e., microstructure in the porous catalyst layer and micro cavities between pellets. However, controllable 3D microstructures, i.e., ordered surface-wise 3D microstructures (see Figure 3e–g) and volume-wise ones (see (g) and (h)) own potential to disentangle and explain interrelated phenomena of heat and mass transfer in the microreactors, and further, can facilitate precise utilization of the precious metal-based catalyst, which ushering in the ultra-low catalyst loading as even thin-film form, i.e., few nanometre-thick catalyst loading.[166] Even though thin-film technology is widely used in microelectronics or microsystems technology, its application on thermocatalysis has been proven in a few recent studies.[166–168] Its interests are not just limited in highly sensitive measurements of catalyst activity and surface kinetics,[168,169] but also in FTS process,[170] CO_2 hydrogenation to methanol,[171] acetylene hydrogenation,[166,168] and dry methane reforming.[172,173] The main attractive advantage of thin-film catalysts is that they enable precise control of the catalyst composition, or the possibility to promote a specific morphology combined with the high degree of

Table 7. FTS kinetic and selectivity models and their areas of application.

Refs.	Kinetic model/Selectivity model	Evaluation of model
FTS selectivity[63,71]	$-r_n = \frac{k_n P_{H_2} P_{CO}^{\beta_n}}{(1+K_{CO}P_{CO})^2}$ $\beta_n = 1\ (n < 5),\ \beta_n = 1.2\ (n \geq 5)$	•Catalyst: 20%Co0.5%Re/γ- Al_2O_3 •Kinetic mechanism: L-H rate expression •Kinetic data were obtained from wash-coated microreactors: monolith (thickness 20 [μm]), micromonolith (thickness 13 [μm]), foam (thickness 55 [μm]), microchannel block (thickness 35 [μm]). •Test conditions: 220–250 [°C], 5–20 [atm], $H_2/CO = 1.5–2.5$, CO conversion < 50% •Compared with experimental temperature distribution along the length, prediction was about 5 °C higher than the measurement.
FTS reaction rate [79,80]	$-r_{CO+H_2} = 0.097 N_{H_2}^{1.25} N_{CO}^{1.3}$	•Catalyst: 16%Co/Al_2O_3(Si) •Kinetic mechanism: empirical model, products are calculated based on material balance •Kinetic data were obtained from a microchannel reactor. •Test conditions: 280–320 [°C], 1–20 [bar], $H_2/CO = 1.4–1.6$, 900–2100 [ml·g_{cat}^{-1}·h^{-1}] •Simulation agreed well with the parts of the experimental data but contradicted the rest.
FTS reaction rate[8,151]	$-r_{CO} = \frac{k P_{H_2}^{0.5} P_{CO}^{0.5}}{(1+K_{CO}P_{CO}^{0.5})^2}$ $-r_{CO} = \frac{k P_{CO} P_{H_2}^{0.5}}{(1+K_{CO}P_{CO})^2}$ $-r_{CO} = \frac{k P_{CO} P_{H_2}}{(1+K_{CO}P_{CO})^2}$	•Catalyst: Co/MgO on SiO_2 •Kinetic mechanism: L-H rate expression •Kinetic data were obtained from a well-mixed continuous-flow slurry reactor. •Test conditions: 220–240 [°C], 0.5–1.5 [MPa], $H_2/CO = 1.5–3.5$ •This model was applied in a tubular packed-bed reactor with internals (diameter 50 [mm], length 1 [m]).[8] Compared with experimental data, prediction was 2–5 [°C] higher than the measurement.
FTS reaction rate[151–153]	$-r_{CO} = \frac{k P_{H_2} P_{CO}}{(1+K_{H_2}P_{H_2}+K_{CO}P_{CO})^2}$	•Catalyst: 12.4%Co/SiO_2 •Kinetic mechanism: L-H rate expression •Kinetic data were obtained from 1-L CSTR.[151,153] •Test conditions: 210 [°C], 2.21 [MPa], $H_2/CO = 1–2.4$, CO conversion 10–70%
FTS reaction rate[107,154]	$-r_{CO} = FkC_{H_2}$	•Catalyst: iron and cobalt-based catalyst, particle size 0.2–2.6 [mm] (large internal diffusion limitation) •Kinetic mechanism: first-order rate expression •Kinetic data were obtained from a fixed-bed microreactor.[154] •Test conditions: 200–250 [°C], 3.1 [MPa], $H_2/CO = 1\&2$, CO conversion < 60%[154] •No validation for the mathematical model
FTS selectivity[10,62,155–157]	$r_{C_1} = k_{C_1} r_{FT}$ $r_{C_2} = k_{C_2} r_{FT}$ $r_{C_n} = \alpha r_{C_{n-1}}\ (n \geq 3)$ $r_{FT} = \frac{k_1 C_{CO} C_{H_2}}{(1+k_2 C_{CO})^2}$	•Catalyst: 12%Co/Al_2O_3, particle size 53–90 [μm] •Kinetic mechanism: $r_{C1\text{-}2}$: Arrhenius law; $r_{Cn\geq 3}$: Anderson–Schultz–Flory (ASF) theory[158,159] with fixed α; r_{FT}: L-H rate expression •Kinetic data were obtained from a steady state isotopic transient kinetic analysis (SSITKA) apparatus.[155–157] •Test conditions: 100–210 [°C], 1.85 [bar], H_2/CO/inert = 15/1.5/33.5 [Nml·min^{-1}][155–157] •No validation for the mathematical model
FTS selectivity[39,73,160]	$S_{c_1}(x,y) = \frac{[1-\alpha(x,y)][1-\alpha(x,y)\cdot(1-\gamma)]}{1-\gamma\alpha(x,y)}$ $S_{c_n}(x,y) = \frac{n[1-\alpha(x,y)]^2\cdot\alpha(x,y)^{n-1}\cdot(1-\gamma)}{1-\gamma\alpha(x,y)}$ $\alpha(x,y) = \frac{1}{1+[\frac{C_{H_2}(x,y)}{C_{CO}(x,y)}]^{\beta}\cdot k_\alpha \cdot \exp[\frac{\Delta E_{a,\alpha}}{R}(\frac{1}{T_{ref}}-\frac{1}{T})]}$	•Catalyst: Co-based catalyst, particle size 1.5 [mm] •Kinetic mechanism: analytic modelling results, mass transfer considered, variable chain growth probability α •Applying conditions: 217 [°C], 30 [bar], $H_2/CO = 1–3$

(*Continued*)

Table 7. (Continued)

Refs.	Kinetic model/Selectivity model	Evaluation of model
FTS selectivity[116,161–163]	$M_n = \frac{\alpha_1^{(n-1)+(\frac{\alpha_1}{\alpha_2})^{(\xi-1)}}\alpha_2^{(n-1)}}{\frac{1}{1-\alpha_1}+(\frac{\alpha_1}{\alpha_2})^{(\xi-1)}(\frac{1}{1-\alpha_2}]}$	•Catalyst: fused magnetite catalyst, particle size 90 [µm] •Kinetic mechanism: 2-α probability distribution, several experimental data are fitted by a modified ASF model •Kinetic data were obtained from a slurry reactor. •Applying range: α_1 = 0.55–0.7, α_2 = 0.8–0.95, ξ = 7
FTS selectivity[105,164,165]	$r_{CH_4} = \frac{k_{CH_4} P_{CO}^{a} P_{H_2}^{b}}{1+\frac{m_{CH_4} P_{H_2O}}{P_{H_2}}}$	•Catalyst: 0.27%Ru–25%Co/Al_2O_3 catalyst, particle size 45–90 [µm] •Kinetic mechanism: empirical power law model •Kinetic data were obtained from a CSTR reactor. •Test conditions: 220 [°C], 1.4–2.5 [MPa], H_2/CO = 1.0–2.5, low CO conversion = 19%
	$r_{C_nH_{2n+2}} = k_1 K_1^{0.5} P_{H_2}^{0.5} \alpha_1 \alpha_2 \prod_{i=3}^{n} \alpha_i [S]^2 \quad n \geq 2$	•Catalyst: 25%Co/0.48%Re/Al_2O_3 •Kinetic mechanism: LHHW approach, CO-insertion mechanism •Kinetic data were obtained from a stirred tank slurry reactor (STSR). •Test conditions: 205, 220 and 230 [°C], 1.5 and 2.5 [MPa], H_2/CO = 1.4 and 2.1
	$r_{C_2H_4} = k_{C_2H_4} e^{c\cdot 2} \alpha_1 \alpha_2 [S]$	
	$r_{C_nH_{2n}} = k_{C_nH_{2n}} e^{c\cdot n} \alpha_1 \alpha_2 \prod_{i=3}^{n} \alpha_i [S] \quad n \geq 3$	

standardization, which might achieve highly selective productivity, though the loading of catalyst will be much lower than packed bed and wash-coated ones. Besides, free internal-mass-transfer resistance and uniform temperature distribution can be easily achieved across the whole catalyst surface. Therefore, proper dimensioning and design of the reactor as well as of the controlled microstructures are quite important to harvest the full potential of the catalyst. Though design strategies based on power catalyst for packed-bed and wash-coated microreactors are summarized in this review, and it may provide as an engineering guide, the design transfer from current experience to the microreactor for thin-film catalyst still requires more investigations.

3.3.2. New Heating/Cooling Concepts

Precise temperature control is critical, especially for the FTS process. The product selectivity and catalyst lifetime are highly dependent on the temperature. Thus, both arrangements of the channels and the heat transfer properties when numbering up microchannel or -tube have drawn quite a lot attention. Amongst many, a few new heating/cooling concepts are reported. Exemplarily, as a cooling strategy, boiling water is proposed as a coolant for highly exothermic processes because the partial boiling condition enables significant heat removal through the enthalpy of vaporization. However, its technical or mechanical challenges are seldomly reported, and the implementation requires further optimization to become applicable for microreactors. For heating strategy, direct current electrical heating of the reactor wall can be facilitated, enabling precise and direct temperature control,[168] which can be quite interesting for low-temperature or endothermal reactions.

3.3.3. Other Design Concepts

Catalyst gradient loading or catalyst positioning and reactant/product removal are also reported in the literature for heat management and variation of the product selectivity.

For catalyst gradient loading/positioning, the activity/mass fraction of the catalyst is intentionally varied along the length of the reactor. This gradient loading can minimize the formation of hot spots by reducing the amount of catalyst especially in the inlet regions, and thus has to date mainly been applied in packed-bed microreactors for highly exothermic processes such as FTS[71] and CO_2 methanation.[86,87] Catalyst positioning has similarly been applied for the auto-thermal for methane SR and methane/air combustion by adjusting the catalyst loading of the endothermic reactions according to the heat evolution from the exothermic reactions or vice versa.[27] However, the main shortcoming of catalyst gradient loading/positioning is the lack of "flexibility", which means one fixed design of loading/positioning in the microreactor is only suitable for a limited range of operating conditions. The change of the flow rate moves the position of the hot spot or changes the temperature distribution, thus, in the worst case, the non-uniformity of the temperature distribution may be aggravated. Inspired by this idea, gradient catalyst thickness/composition, gradient microstructure, gradient hydraulic diameter, etc., could also be envisioned for specific challenges.

On the other hand, varying the position of the reactant feed and/or product removal during the catalytic process along the reactor may be used to deliberately shift the reaction's thermodynamic equilibrium using membrane reactors.[174] For example, CO_2 methanation (Sabatier process) is a reversible reaction in which water removal shifts the equilibrium to favor the production of more methane. The optimal position for product removal is determined by various factors, and similarly, the effectiveness of such design is limited to a certain range of operation conditions.

4. Conclusion

A catalogue of experiences from experiments and simulations for engineering design strategies of different types of microreactors to achieve negligible temperature and concentration gradients as well as low pressure drop and narrow residence time distribution, is growing. However, globally valid design principles of geometry and dimension in terms of reactors as well as microstructures in the reactor for tuning the catalytic selectivity are still lacking. In this review, design parameters of microreactors and their implications on the reactor's performance are compiled and discussed in the context of the FTS process. Guidelines for the consideration of proper dimensions, geometry, materials, catalyst arrangement, and microstructures in the reactor are provided to optimize heat and mass transfer, pressure drop and residence time distribution. Recommendations for the catalyst loading of packed-bed and wash-coated microchannel, microtube, micromonolith and microstructured reactors are summarized. Additionally, the transferability of design boundaries on FTS to other syngas processes is also discussed. It is noticed that design strategies in terms of heat transfer, mass transfer, pressure drop, and residence time distribution may exist conflicts; however, reconciliation needs to be made to achieve specific product selectivity, temperature distribution, and production rate.

The scalability of microreactors allows to realize a variety of large-scale applications from lab-scale instigations. It is envisioned that the favorable process intensifying characteristics of microreactors will be implemented at the pilot- and commercial scale of microchannel-based design via numbering up methods.

In particular, microstructure has been found to be able to enhance heat and mass transfer, adjust flow profiles, decrease pressure drop, and increase catalyst inventory, and it has become one of the key design aspects for microreactors. A growing interest in controllable micro-structuring of both the reactor surface and catalyst, instead of using random catalyst packing and unpredictable powder porous structure, has been shown. With microstructuring, the applicability and adaptability of microreactors as well as the tunability of operation parameters, can be enlarged.

Finally, as the microreactors for FTS is one of today's hot topics in the reaction engineering community, although clear design methodologies are not scoped, we hope that this review can serve as a practical summary and comprehensive overview of the microreactor design. Together with the ongoing efforts in microstructuring investigations, microreactors for catalytic reactions might not be regarded as "micro size" but instead as an emerging energy-renewable solution.

Acknowledgements

The authors acknowledge support from the German Federal Ministry of Education and Research in the framework of the project Catlab (Grant No. 03EW0015A).

Conflict of Interest

The authors declare no conflict of interest.

Keywords

design, Fischer–Tropsch, heat transfer, mass transfer, microreactor, process intensification

Received: July 22, 2025
Revised: October 15, 2025
Published online: November 4, 2025

[1] U.S. Energy Information Administration, International Energy Outlook 2023, https://www.eia.gov/outlooks/ieo/ **2023** (accessed: October 2025).
[2] European Council, The 2030 climate and energy framework, https://www.consilium.europa.eu/en/policies/climate-change/2030-climate-and-energy-framework/ **2017** (accessed: October 2025).
[3] P. D. Lund, J. Lindgren, J. Mikkola, J. Salpakari, *Renew. Sustain. Energy Rev.* **2015**, *45*, 785.
[4] C. Sun, P. Pfeifer, R. Dittmeyer, *Chem. Eng. J.* **2017**, *326*, 37.
[5] Z. Gholami, Z. Tišler, V. Rubáš, *Catal. Rev.* **2021**, *63*, 512.
[6] S. Saeidi, M. Talebi Amiri, N. A. Saidina Amin, M. R. Rahimpour, *Int. J. Chem. React. Eng.* **2014**, *12*, 639.
[7] J. Xu, Y. Yang, Y.-W. Li, *Energy and environmental engineering /Reaction engineering and catalysis* **2013**, *2*, 354.
[8] J. Shen, W. H. Ho, X. Liu, D. Hildebrandt, *Chem. Eng. Process. Process Intensif.* **2021**, *161*, 108309
[9] J. W. Pratt, A Fischer–Tropsch Synthesis Reactor Model Framework for Liquid Biofuels Production **2012**.
[10] G. Chabot, R. Guilet, P. Cognet, C. Gourdon, *Chem. Eng. Sci.* **2015**, *127*, 72.
[11] M. Sadeqzadeh, J. Hong, P. Fongarland, D. Curulla-Ferré, F. Luck, J. Bousquet, D. Schweich, A. Y. Khodakov, *Ind. Eng. Chem. Res.* **2012**, *51*, 11955.
[12] F. Meng, M. A. Nawaz, *Advances in Slurry Technology* (Ed. T. Frank Jones), IntechOpen, Rijeka **2022**.
[13] S. R. Deshmukh, A. L. Y. Tonkovich, K. T. Jarosch, L. Schrader, S. P. Fitzgerald, D. R. Kilanowski, J. J. Lerou, T. J. Mazanec, *Ind. Eng. Chem. Res.* **2010**, *49*, 10883.
[14] J. Na, K. S. Kshetrimayum, I. Jung, S. Park, Y. Lee, O. Kwon, Y. Mo, J. Chung, J. Yi, U. Lee, C. Han, *Chem. Eng. Process. Process Intensif.* **2018**, *128*, 63.
[15] Y. Woo, D. B. Oh, J. E. Park, S. J. Han, Y.-J. Lee, M.-J. Park, *Korean J. Chem. Eng.* **2023**.
[16] P. Pfeifer, S. Schmidt, F. Betzner, M. Kollmann, M. Loewert, T. Böltken, P. Piermartini, *Curr. Opin. Chem. Eng.* **2022**, *36*, 100776.
[17] Y. Ganjkhanlou, E. Boymans, B. Vreugdenhil, *Fuels* **2025**, *6*, 24.
[18] J. E. Apolinar-Hernández, S. L. Bertoli, H. G. Riella, C. Soares, N. Padoin, *Energy Fuels* **2024**, *38*, 1.
[19] P. Piermartini, T. Boeltken, M. Selinsek, P. Pfeifer, *Chem. Eng. J.* **2017**, *313*, 328.
[20] A. Holmen, H. J. Venvik, R. Myrstad, J. Zhu, C. De, *SI: ICOSCAR-4* **2013**, *216*, 150.

[21] C. Cao, J. Hu, S. Li, W. Wilcox, Y. Wang, *Chemicals and Petrochemicals* **2009**, *140*, 149.
[22] Z. Teimouri, N. Abatzoglou, A. K. Dalai, *Catalysts* **2021**, *11*, 330.
[23] H. Jahangiri, J. Bennett, P. Mahjoubi, K. Wilson, S. Gu, *Catal. Sci. Technol.* **2014**, *4*, 2210.
[24] Y. Suo, Y. Yao, Y. Zhang, S. Xing, Z.-Y. Yuan, *J. Ind. Eng. Chem.* **2022**, *115*, 92.
[25] N. H. Naqiuddin, L. H. Saw, M. C. Yew, F. Yusof, T. C. Ng, M. K. Yew, *Renew. Sustain. Energy Rev.* **2018**, *82*, 901.
[26] P. L. Suryawanshi, S. P. Gumfekar, B. A. Bhanvase, S. H. Sonawane, M. S. Pimplapure, *Chem. Eng. Sci.* **2018**, *189*, 431.
[27] N. Engelbrecht, R. C. Everson, D. Bessarabov, G. Kolb, *Chem. Eng. Process. Process Intensif.* **2020**, *157*, 108164.
[28] L. He, Y. Fan, J. Bellettre, J. Yue, L. Luo, *Renew. Sustain. Energy Rev.* **2020**, *119*, 109589.
[29] Z. Dong, Z. Wen, F. Zhao, S. Kuhn, T. Noël, *Chemical Engineering Science: X* **2021**, *10*, 100097.
[30] M. Harris, H. Wu, W. Zhang, A. Angelopoulou, *Chem. Eng. Process. Process Intensif.* **2022**, *181*, 109155.
[31] Z. Teimouri, V. B. Borugadda, A. K. Dalai, N. Abatzoglou, *Renew. Sustain. Energy Rev.* **2022**, *160*, 112287.
[32] D. Yadav, X. Lu, B.-C. Ma, D. Jing, *J. Power Sources* **2024**, *596*, 234090.
[33] A. L. Y. Tonkovich, B. Yang, S. T. Perry, S. P. Fitzgerald, Y. Wang, *The Novel Compact Catalytic Reactor* **2007**, *120*, 21.
[34] Bo Leckner, P. Szentannai, F. Winter, *Fuel* **2011**, *90*, 2951.
[35] J. Sternéus, F. Johnsson, B. Leckner, *Powder Technol.* **2002**, *126*, 28.
[36] D. G. Vlachos, in *Microfabricated Power Generation Devices: Design and Technology* (Eds. A. Mitsos, P. I. Barton), Wiley-VCH Verlag GmbH & Co. KGaA, Weinheim, **2009**, pp. 179–198.
[37] P.-F. Hao, Z.-H. Yao, F. He, Ke-Q Zhu, *J. Micromech. Microeng.* **2006**, *16*, 1397.
[38] C. D. Park, T. Nosoko, S. Gima, S. T. Ro, *Int. J. Heat Mass Transfer* **2004**, *47*, 2587.
[39] D. Vervloet, F. Kapteijn, J. Nijenhuis, J. R Van Ommen, *Catal. Sci. Technol.* **2012**, *2*, 1221.
[40] Octave Levenspiel *Tracer Technology. Fluid Mechanics and Its Applications*, Springer, New York, NY, **2012**.
[41] H Scott Fogler *Elements of Chemical Reaction Engineering*, Prentice Hall PTR, New Jersey, **2006**.
[42] *Octave Levenspiel Chemical Reaction Engineering*, John Wiley and Sons, New York, **1998**.
[43] D. E. Mears, *Ind. Eng. Chem. Fundam.* **1971**, *10*, 541.
[44] M. Mandić, B. Todić, L. Živanić, N. Nikačević, D. B. Bukur, *Ind. Eng. Chem. Res.* **2017**, *56*, 2733.
[45] A. Aguirre, V. Chandra, E. A. J. F. Peters, J. A. M. Kuipers, M. F. Neira D'Angelo, *Chem. Eng. J.* **2020**, *393*, 124656.
[46] B. Leckner, J. Werther, *Energy Fuels* **2000**, *14*, 1286.
[47] A. Gómez-Barea, B. Leckner, *Prog. Energy Combust. Sci.* **2010**, *36*, 444.
[48] S. Ergun, A. A. Orning, *Chem. Eng. Prog.* **1949**, *41*, 1179.
[49] S. Hofmann, A. Bufe, G. Brenner, T. Turek, *Chem. Eng. Sci.* **2016**, *155*, 376.
[50] N. Kockmann, *Chem. Eng. Technol.* **2008**, *31*, 1188.
[51] Li Zhang, H. Chu, H. Qu, Qi Zhang, H. Xu, J. Cao, Z. Tang, J. Xuan, *Int. J. Hydrogen Energy* **2018**, *43*, 3077.
[52] P. Gunnasegaran, H. A. Mohammed, N. H. Shuaib, R. Saidur, *Int. Commun. Heat Mass Transf.* **2010**, *37*, 1078.
[53] A. Fazeli, M. Behnam, *Int. J. Hydrogen Energy* **2010**, *35*, 9496.
[54] L. He, Y. Fan, J. Bellettre, J. Yue, L. Luo, *Chem. Eng. Sci.* **2021**, *236*, 116517.
[55] W. Lu, R. Zhang, S. Toan, R. Xu, F. Zhou, Z. Sun, Z. Sun, *Chem. Eng. J.* **2022**, *429*, 132286.
[56] H. A. Mohammed, P. Gunnasegaran, N. H. Shuaib, *Int. Commun. Heat Mass Transf.* **2011**, *38*, 63.
[57] Y. Zhai, G. Xia, Z. Chen, Z. Li, *Int. J. Heat Mass Transfer* **2016**, *98*, 380.
[58] D. H. West, V. Balakotaiah, Z. Jovanovic, *Environmental Catalysis and Reaction Engineering* **2003**, *88*, 3.
[59] S. Y. Joshi, M. P. Harold, V. Balakotaiah, *Chem. Eng. Sci.* **2010**, *65*, 1729.
[60] V. Balakotaiah, D. H. West, *Chem. Eng. Sci.* **2002**, *57*, 1269.
[61] M. Ibáñez, O. Sanz, A. Egaña, I. Reyero, F. Bimbela, L. M. Gandía, M. Montes, *Chem. Eng. J.* **2021**, *425*, 130424.
[62] R. Philippe, M. Lacroix, L. Dreibine, C. Pham-Huu, D. Edouard, S. Savin, F. Luck, D. Schweich, *Catal. Today* **2009**, *147*, S305.
[63] L. C. Almeida, O. Sanz, D. Merino, G. Arzamendi, L. M. Gandía, M. Montes, *Catalysis and Synthetic Fuels: State of the Art and Outlook* **2013**, *215*, 103.
[64] D. Vervloet, F. Kapteijn, J. Nijenhuis, J. Ruud van Ommen, *SI: ICOSCAR-4* **2013**, *216*, 111.
[65] B. Kaskes, D. Vervloet, F. Kapteijn, J. R. van Ommen, *Chem. Eng. J.* **2016**, *283*, 1465.
[66] L. L. Makarshin, Z. P. Pai, V. N. Parmon, *Russ. Chem. Rev.* **2016**, *85*, 139.
[67] Z. Wang, J. Gao, K. Chang, L. Meng, N. Zhang, Z. Guo, *RSC Adv.* **2018**, *8*, 15933.
[68] Gemini, Knitted Column Packing, https://www.geminiwiremesh.org/product/knitted-column-packing/ (accessed: October 2025).
[69] S. R. A. Ruth, L. Beker, H. Tran, V. R. Feig, N. Matsuhisa, Z. Bao, *Adv. Funct. Mater.* **2020**, *30*, 1903100.
[70] V. Meille, S. Pallier, G. V. Santa Cruz Bustamante, M. Roumanie, J.-P. Reymond, *Appl. Catal., A* **2005**, *286*, 232.
[71] X. Wang, Y. Ren, Li Zhang, *Chem. Eng. J.* **2023**, *452*, 139188.
[72] J. Knochen, R. Güttel, C. Knobloch, T. Turek, *Chem. Eng. Process.: Process Intensif.* **2010**, *49*, 958.
[73] H. Becker, R. Güttel, T. Turek, *Catal. Sci. Technol.* **2019**, *9*, 2180.
[74] K. Ramanathan, V. Balakotaiah, D. H. West, *AIChE J.* **2004**, *50*, 1493.
[75] U. Tozar, A. K. Avci, *Chem. Eng. Process. Process Intensif.* **2020**, *151*, 107914.
[76] M. Zanfir, M. Baldea, P. Daoutidis, *AIChE J.* **2011**, *57*, 2518.
[77] M. I. Hosukoglu, M. Karakaya, A. K. Avci, *Ind. Eng. Chem. Res.* **2012**, *51*, 8913.
[78] O. Tonomura, M. Noda, S. Hasebe, *Front. Chem. Eng.* **2022**, *4*.
[79] A. Rai, M. Anand, S. A. Farooqui, M. G. Sibi, A. K. Sinha, *React. Chem. Eng.* **2018**, *3*, 319.
[80] A. Rai, M. G. Sibi, S. A. Farooqui, M. Anand, A. Bhaumik, A. K. Sinha, *ACS Sustainable Chem. Eng.* **2017**, *5*, 7576.
[81] A. J. L. Foong, N. Ramesh, T. T. Chandratilleke, *Int. J. Therm. Sci.* **2009**, *48*, 1908.
[82] E. S. Cho, J. W. Choi, J. S. Yoon, M. S. Kim, *Int. J. Heat Mass Transfer* **2010**, *53*, 1341.
[83] V. V. Dharaiya, S. G. Kandlikar, *Int. J. Heat Mass Transfer* **2013**, *57*, 190.
[84] J.-S. Park, D.-E. Kim, Y.-J. Lee, G. Kwak, K.-W. Jun, M.-J. Park, *Ind. Eng. Chem. Res.* **2016**, *55*, 9416.
[85] I. Jung, J. Na, S. Park, J. Jeon, Y-Gi Mo, J.-Y. Yi, J.-T. Chung, C. Han, *Fuel Process. Technol.* **2017**, *159*, 448.
[86] F. Kosaka, T. Yamaguchi, Y. Ando, T. Mochizuki, H. Takagi, K. Matsuoka, K. Kuramoto, *Int. J. Hydrogen Energy* **2021**, *46*, 4116.
[87] F. Kosaka, T. Yamaguchi, Y. Ando, T. Mochizuki, H. Takagi, K. Matsuoka, Y. Fujishiro, K. Kuramoto, *Int. J. Hydrogen Energy* **2020**, *45*, 12911.
[88] K. S. Kshetrimayum, I. Jung, J. Na, S. Park, Y. Lee, S. Park, C.-J. Lee, C. Han, *Ind. Eng. Chem. Res.* **2016**, *55*, 543.
[89] R. Güttel, *Chem. Ing. Tech.* **2015**, *87*, 694.
[90] D. Copiello, G. Fabbri, *Int. J. Heat Mass Transfer* **2009**, *52*, 1167.
[91] R. Myrstad, S. Eri, P. Pfeifer, E. Rytter, A. Holmen, *Catal. Today* **2009**, *147*, S301.
[92] M. Karakaya, A. K. Avci, *Int. J. Hydrogen Energy* **2011**, *36*, 6569.
[93] G. Gumuslu, A. K. Avci, *AIChE J.* **2012**, *58*, 227.
[94] G. Arzamendi, P. M. Diéguez, M. Montes, J. A. Odriozola, E. Falabella Sousa-Aguiar, L. M. Gandía, *Chem. Eng. J.* **2010**, *160*, 915.

[95] N. Kockmann, M. Gottsponer, D. M. Roberge, *Chem. Eng. J.* **2011**, *167*, 718.
[96] M. Loewert, J. Hoffmann, P. Piermartini, M. Selinsek, R. Dittmeyer, P. Pfeifer, *Chem. Eng. Technol.* **2019**, *42*, 2202.
[97] D. Liu, X. Chen, *Combust. Flame* **2010**, *157*, 2116.
[98] A. Gómez-Barea, B. Leckner, D. Santana, P. Ollero, *Chem. Eng. J.* **2008**, *141*, 151.
[99] H. J. Merk, *Appl. Sci. Res., Sect. A* **1959**, *8*, 73.
[100] J. Wentrup, G. R. Pesch, J. Thöming, *Renew. Sustain. Energy Rev.* **2022**, *162*, 112454.
[101] A. Duerksen, J. Thiessen, C. Kern, A. Jess, *Sustain. Energy Fuels* **2020**, *4*, 2055.
[102] E. Rytter, A. Holmen, *Catalysts* **2015**, *5*, 478.
[103] Y. Sun, Z. Jia, G. Yang, L. Zhang, Z. Sun, *Int. J. Hydrogen Energy* **2017**, *42*, 29222.
[104] N. Mohammad, S. Bepari, S. Aravamudhan, D. Kuila, *Catalysts* **2019**, *9*, 872.
[105] H. Cao, R. Xu, X. Tang, T. Yang, S. Hou, C. Hou, *Chin. J. Chem. Eng.* **2023**, *64*, 224.
[106] M. Stamenić, V. Dikić, M. Mandić, B. Todić, D. B. Bukur, N. M. Nikačević, *Ind. Eng. Chem. Res.* **2017**, *56*, 9964.
[107] R. Guettel, T. Turek, *Chem. Eng. Sci.* **2009**, *64*, 955.
[108] A. Aguirre, E. Scholman, J. Van Der Shaaf, M. F Neira d'Angelo, *Chem. Eng. J.* **2021**, *409*, 128139.
[109] B. Xu, Y. Fan, Y. Zhang, N. Tsubaki, *AIChE J.* **2005**, *51*, 2068.
[110] O. Borg, S. Eri, E. Blekkan, S. Storsater, H. Wigum, E. Rytter, A. Holmen, *J. Catal.* **2007**, *248*, 89.
[111] A. Y. Khodakov, A. Griboval-Constant, R. Bechara, V. L. Zholobenko, *J. Catal.* **2002**, *206*, 230.
[112] A. M. Saib, M. Claeys, E. van Steen, *Fischer–Tropsch synthesis on the eve of the XXI Century* **2002**, *71*, 395.
[113] H. Preising, D. Enke, *Colloids Surf. A* **2007**, *300*, 21.
[114] C. K. Colton, C. N. Satterfield, C.-J. Lai, *AIChE J.* **1975**, *21*, 289.
[115] M. C. Tsai, Y. W. Chen, C. Li, *Ind. Eng. Chem. Res.* **1993**, *32*, 1603.
[116] N. Mohammad, C. Chukwudoro, S. Bepari, O. Basha, S. Aravamudhan, D. Kuila, *Catal. Today* **2022**, *397–399*, 182.
[117] H. Becker, R. Güttel, T. Turek, *Catal. Sci. Technol.* **2016**, *6*, 275.
[118] C. Y. Lee, C. R. Wilke, *Ind. Eng. Chem.* **1954**, *46*, 2381.
[119] C. Kern, A. Jess, *Energy Technol.* **2024**, *12*, 2301534.
[120] E. L. C. Seris, G. Abramowitz, A. M. Johnston, B. S. Haynes, *Chem. Eng. J.* **2008**, *135*, S9.
[121] R. K. Thakur, Ch. Vial, K. D. P. Nigam, E. B. Nauman, G. Djelveh, *Chem. Eng. Res. Des.* **2003**, *81*, 787.
[122] C. Knobloch, R. Güttel, T. Turek, *Chem. Ing. Tech.* **2013**, *85*, 455.
[123] D. Bošković, S. Loebbecke, *Chem. Eng. J.* **2008**, *135*, S138.
[124] P. Orth, K. Schügerl, *Chem. Eng. Sci.* **1972**, *27*, 497.
[125] J. Aubin, L. Prat, C. Xuereb, C. Gourdon, *Chem. Eng. Process.: Process Intensif.* **2009**, *48*, 554.
[126] A. Rafiee, M. Hillestad, *Chem. Eng. Technol.* **2013**, *36*, 1729.
[127] B. Kaskes, D. Vervloet, F. Kapteijn, J. R. van Ommen, *Ind. Eng. Chem. Res.* **2014**, *53*, 16579.
[128] D. Vervloet, M. R. Kamali, J. J. J. Gillissen, J. Nijenhuis, H. E. A. Van Den Akker, F. Kapteijn, J. R. Van Ommen, *Catal. Today* **2009**, *147*, S138.
[129] A. Theampetch, W. Chaiwang, N. Jermkwan, P. Narataruksa, T. Sornchamni, C. Prapainainar, *Energy Procedia* **2016**, *100*, 439.
[130] U. Roy, P. K. Roy, *Advanced Analytic and Control Techniques for Thermal Systems with Heat Exchangers*, (Ed. L. Pekař), Academic Press, New York, United States, **2020**, pp. 197.
[131] R. Güttel, T. Turek, *Energy Technol.* **2016**, *4*, 44.
[132] C. V. Ovesen, B. S. Clausen, J. Schiøtz, P. Stoltze, H. Topsøe, J. K. Nørskov, *J. Catal.* **1997**, *168*, 133.
[133] M. Peter, M. B. Fichtl, H. Ruland, S. Kaluza, M. Muhler, O. Hinrichsen, *Chem. Eng. J.* **2012**, *203*, 480.
[134] T. Van Herwijnen, H. Van Doesburg, W. A. De Jong, *J. Catal.* **1973**, *28*, 391.
[135] J. Klose, *J. Catal.* **1984**, *85*, 105.
[136] C. V. Miguel, A. Mendes, L. M. Madeira, *J. CO2 Util.* **2018**, *25*, 128.
[137] M. Niwa, K. Awano, Y. Murakami, *Appl. Catal.* **1983**, *7*, 317.
[138] D. L. Trimm, C.-W. Lam, *Chem. Eng. Sci.* **1980**, *35*, 1405.
[139] J. Na, K. S. Kshetrimayum, U. Lee, C. Han, *Chem. Eng. J.* **2017**, *313*, 1521.
[140] S. Arab, J.-M. Commenge, J.-F. Portha, L. Falk, *Chem. Eng. Res. Des.* **2014**, *92*, 2598.
[141] Y. Wang, Y. H. Chin, R. T. Rozmiarek, B. R. Johnson, Y. Gao, J. Watson, A. Y. L. Tonkovich, D. P. Vander Wiel, *Catal. Today* **2004**, *98*, 575.
[142] B. Kucharczyk, W. Tylus, L. Kępiński, *Appl. Catal., B* **2004**, *49*, 27.
[143] L.-h. Xiao, K.-p. Sun, X.-l. Xu, X.-n. Li, *Catal. Commun.* **2005**, *6*, 796.
[144] R. Mutschler, E. Moioli, *Catalysts* **2021**, *11*, 311.
[145] H. Becker, R. Güttel, T. Turek, *Chem. Ing. Tech.* **2014**, *86*, 544.
[146] Y.-N. Wang, Y.-Y. Xu, H.-W. Xiang, Y.-W. Li, B.-J. Zhang, *Ind. Eng. Chem. Res.* **2001**, *40*, 4324.
[147] I. Iliuta, F. Larachi, B. P. A. Grandjean, G. Wild, *Chem. Eng. Sci.* **1999**, *54*, 5633.
[148] R. Krishna, S. T. Sie, *Fuel Process. Technol.* **2000**, *64*, 73.
[149] G. Wild, F. Larachi, J. C. Charpentier, *Heat and Mass Transfer in Gas-Liquid-Solid Fixed Bed Reactors*, Elsevier, Amsterdam, The Netherlands, **1992**.
[150] M. A. Latifi, A. Naderifar, N. Midoux, *Chem. Eng. Sci.* **1997**, *52*, 4005.
[151] I. C. Yates, C. N. Satterfield, *Energy Fuels* **1991**, *5*, 168.
[152] M.-S. Shin, N. Park, M.-J. Park, K.-W. Jun, K.-S. Ha, *Chem. Eng. J.* **2013**, *234*, 23.
[153] T. K. Das, W. A. Conner, J. Li, G. Jacobs, M. E. Dry, B. H. Davis, *Energy Fuels* **2005**, *19*, 1430.
[154] M. F. M. Post, A. C. Van't Hoog, J. K. Minderhoud, S. T. Sie, *AIChE J.* **1989**, *35*, 1107.
[155] M. J. Keyser, R. C. Everson, R. L. Espinoza, *Ind. Eng. Chem. Res.* **2000**, *39*, 48.
[156] S. Storsæter, D. Chen, A. Holmen, *Surf. Sci.* **2006**, *600*, 2051.
[157] V. Frøseth, S. Storsæter, Ø. Borg, E. A. Blekkan, M. Rønning, A. Holmen, *Appl. Catal., A* **2005**, *289*, 10.
[158] P. J. Flory, *J. Am. Chem. Soc.* **1936**, *58*, 1877.
[159] in *The IUPAC Compendium of Chemical Terminology*, International Union of Pure and Applied Chemistry (IUPAC), Zürich, Switzerland **2014**.
[160] D. Förtsch, K. Pabst, E. Groß-Hardt, *Chem. Eng. Sci.* **2015**, *138*, 333.
[161] T. J. Donnelly, I. C. Yates, C. N. Satterfield, *Energy Fuels* **1988**, *2*, 734.
[162] G. A. Huff Jr., C. N. Satterfield, M. H. Wolf, *Ind. Eng. Chem. Fundam.* **1983**, *22*, 258.
[163] G. Huff, *J. Catal.* **1984**, *85*, 370.
[164] B. Todic, W. Ma, G. Jacobs, B. H. Davis, D. B. Bukur, *Natural Gas Conversion the Status and Potentials in the Light of NGCS-10* **2014**, *228*, 32.
[165] W. Ma, G. Jacobs, T. K. Das, C. M. Masuku, J. Kang, V. R. R. Pendyala, B. H. Davis, J. L. S. Klettlinger, C. H. Yen, *Ind. Eng. Chem. Res.* **2014**, *53*, 2157.
[166] Z. Li, E. Öztuna, K. Skorupska, O. V. Vinogradova, A. Jamshaid, A. Steigert, C. Rohner, M. Dimitrakopoulou, M. J. Prieto, C. Kunkel, M. Stredansky, P. Kube, M. Götte, A. M. Dudzinski, F. Girgsdies, S. Wrabetz, W. Frandsen, R. Blume, P. Zeller, M. Muske, D. Delgado, S. Jiang, F.-P. Schmidt, T. Köhler, M. Arztmann, A. Efimenko, J. Frisch, T. M. Kokumai, R. Garcia-Diez, M. Bär, et al., *Nat. Commun.* **2024**, *15*, 10660.
[167] B. Rech, R. Schlögl, *Bunsen-Magazin* **2022**, *3*, 93.
[168] C. Trinh, Y. Wei, A. Yadav, M. Muske, N. Grimm, Z. Li, L. Thum, D. Wallacher, R. Schlögl, K. Skorupska, R. Schlatmann, D. Amkreutz, *Chem. Eng. J.* **2023**, *477*, 146926.

[169] T. R. Henriksen, J. L. Olsen, P. Vesborg, I. Chorkendorff, O. Hansen, *Rev. Sci. Instrum.* **2009**, *80*, 124101.
[170] A. Kunene, Y. Wei, E. V. Steen, M. H. Raza, I. E. Arrouji, C. E. Jiménez, R. Félix, D. Toebbens, A. S. Malik, V. Padayachee, D. D. Oliveira, M. Fadlalla, M. Bär, S. Calnan, M. Claeys, R. Schlatmann, D. Amkreutz, Thin-Film Catalysis Innovations in Fischer–Tropsch Synthesis for Enhanced Activity, **2025**.
[171] S. Shivam, M. Javed, G. Brösigke, J.-U. Repke, L. Thum, R. Van De Krol, I. Lauermann, R. Schlatmann, A. Gili, D. Amkreutz, *Adv. Funct. Mater.* **2025**, *35*, 14003.
[172] R. Rezaei, G. Moradi, *Int. J. Hydrogen Energy* **2018**, *43*, 21374.
[173] M. Moradi, G. Moradi, A. Heydarinasab, A. Rashidi, *Mater. Today Commun.* **2023**, *34*, 105226.
[174] S. E. Hashemi, K. M. Lien, M. Hillestad, S. K. Schnell, B. Austbø, *Energies* **2021**, *14*, 7861.

Yangjun Wei is a Postdoctoral Fellow at Helmholtz Zentrum Berlin (Germany). She received a Ph.D. from Zhejiang University (China) in 2022. Her research focuses on reactor design and multiscale modeling.

Lukas Thum studied chemistry at the Technical University of Berlin (Germany) and received his Ph.D. in 2020. He then worked as a post-doctoral researcher at the Fritz Haber Institute of the Max Planck Society (Germany). Since 2023 he is a post-doctoral researcher at the Helmholtz-Zentrum Berlin (Germany). His research interest focusses on heterogeneous catalysis, including reaction engineering, kinetic modelling and catalyst development.

Avela Kunene is a Postdoctoral Fellow at Helmholtz Zentrum Berlin (HZB) -Germany. She holds a Ph.D. in Chemical Engineering from the University of Cape Town (South Africa). Her research interests lie in thermal catalysis, with particular emphasis on Fischer-Tropsch synthesis, liquid fuel synthesis from biomass, and the alcohol oxidation reaction.

Daniel Amkreutz is head of the group thin-film catalysts & reactors for sustainable fuels at Helmholtz-Zentrum Berlin, Institute PVcomB. He received his Ph.D. in 2011 from Hamburg University of Technology (TUHH) in the field of thin-film solar cells. His research group focuses on the development and characterisation of thin-film materials for thermocatalysis in the field of energy conversion and storage. The work includes the development and optimisation of thin-film catalyst systems, 2D/3D substrate modifications, characterisation of the morphological, mechanical and electronic properties and the development of screening- and thermocatalytic reactor concepts for the chemical validation of the developed catalyst systems.

Rutger Schlatmann is the founding director of the technology transfer institute PVcomB at the Helmholtz-Zentrum Berlin (HZB), where he is also the head of the solar energy division. Since 2022, he is the elected Chair of the European Technology & Innovation Platform Photovoltaics, a high-level advisory body to the European Commission. Since 2020, he has been the speaker of the topic Photovoltaics and Wind within the Helmholtz Association, combining the programs for HZB, Forschungszentrum Juelich, Karlsruhe Institute of Technology and DLR. Since 2012, he has been a full professor Photovoltaic Technology HTW Berlin Before returning to academia in 2008, he worked in industry for 12 years, first as a staff scientist Akzo Nobel corporate research and from 1999 until 2008 as R&D manager at solar cell company Hyet Solar (formerly Helianthos, daughter company AkzoNobel/Shell Solar/Nuon).

Sonya Calnan joined Loughborough University, UK in July 2024 as a full professor of Energy Engineering in the Wolfson School of Mechanical, Electrical and Manufacturing Engineering. Prior to that, she led the Photovoltaics to Fuels Technology research group at the Helmholtz-Zentrum Berlin, Germany. Her research interests include chemical reactors and process development for energy and fuels conversion using hydrogen and its derivatives.